molecules

MDPI

Article

Characterization of Copper(II) and Zinc(II) Complexes of Peptides Mimicking the CuZnSOD Enzyme

Enikő Székely, Mariann Molnár, Norbert Lihi and Katalin Várnagy *

Department of Inorganic and Analytical Chemistry, University of Debrecen, Egyetem Square 1, H-4032 Debrecen, Hungary

* Correspondence: varnagy.katalin@science.unideb.hu; Tel.: +36-52-512-900

Abstract: Antimicrobial peptides are short cationic peptides that are present on biological surfaces susceptible to infection, and they play an important role in innate immunity. These peptides, like other compounds with antimicrobial activity, often have significant superoxide dismutase (SOD) activity. One direction of our research is the characterization of peptides modeling the CuZnSOD enzyme and the determination of their biological activity, and these results may contribute to the development of novel antimicrobial peptides. In the framework of this research, we have synthesized 10, 15, and 16-membered model peptides containing the amino acid sequence corresponding to the Cu(II) and Zn(II) binding sites of the CuZnSOD enzyme, namely the Zn(II)-binding HVGD sequence (80–83. fragments), the Cu(II)-binding sequence HVH (fragments 46–48), and the histidine (His63), which links the two metal ions as an imidazolate bridge: Ac-FHVHEGPHFN-NH_2 (L^1(10)), Ac-FHVHAGPHFNGGHVG-NH_2 (L^2(15)), and Ac-FHVHEGPHFNGGHVGD-NH_2 (L^3(16)). pH-potentiometric, UV-Vis-, and CD-spectroscopy studies of the Cu(II), Zn(II), and Cu(II)-Zn(II) mixed complexes of these peptides were performed, and the SOD activity of the complexes was determined. The binding sites preferred by Cu(II) and Zn(II) were identified by means of CD-spectroscopy. From the results obtained for these systems, it can be concluded that in equimolar solution, the –(NGG)HVGD- sequence of the peptides is the preferred binding site for copper(II) ion. However, in the presence of both metal ions, according to the native enzyme, the -HVGD- sequence offers the main binding site for Zn(II), while the majority of Cu(II) binds to the -FHVH- sequence. Based on the SOD activity assays, complexes of the 15- and 16-membered peptide have a significant SOD activity. Although this activity is smaller than that of the native CuZnSOD enzyme, the complexes showed better performance in the degradation of superoxide anion than other SOD mimics. Thus, the incorporation of specific amino acid sequences mimicking the CuZnSOD enzyme increases the efficiency of model systems in the catalytic decomposition of superoxide anion.

Keywords: multihistidine peptide; Cu(II)-complex; Zn(II)-complex; SOD activity; CuZnSOD

Citation: Székely, E.; Molnár, M.; Lihi, N.; Várnagy, K. Characterization of Copper(II) and Zinc(II) Complexes of Peptides Mimicking the CuZnSOD Enzyme. *Molecules* **2024**, *29*, 795. https://doi.org/10.3390/molecules29040795

Academic Editors: Denise Bellotti and Maurizio Remelli

Received: 29 December 2023
Revised: 1 February 2024
Accepted: 1 February 2024
Published: 8 February 2024

1. Introduction

The superoxide anion, O_2^-, is produced by the one-electron reduction of dioxygen in numerous biochemically relevant redox processes [1]. These very toxic species are thought to play a role in diseases and pathological processes, such as aging, cancer, or membrane or DNA damage, etc. [2]. Cells are protected against this species by superoxide dismutase (SOD)—a metalloenzyme, which very efficiently catalyzes the dismutation of superoxide anion into H_2O_2 and O_2. With this reaction, SOD reduces the risk of oxidative stress by eliminating the highly reactive superoxide [3]. In addition, SOD1 mutations are associated with human familial amyotrophic lateral sclerosis (ALS) [4,5]. SODs are also expected to play a role in modulating innate immunity, as O_2 is one of several toxic substances used by the cellular arm of the immune system to kill bacteria and virus-infected cells [6,7]. CuZnSODs are metalloproteins whose structure is provided by a zinc atom, and a copper atom is the catalytic cofactor [8]. In vivo, the zinc atom is likely to be transported to the

enzyme by passive diffusion, while the copper atom is transported by a copper chaperone via a translocation mechanism in a process that requires the formation of a SOD-copper chaperone heterodimer [9–13].

Antimicrobial peptides are short cationic peptides that are present on biological surfaces susceptible to infection and play an important role in innate immunity [14]. A very large number of different antimicrobial peptides have been discovered. Many antimicrobial peptides are characterized by an amphipathic structure [15]. Antimicrobial peptides include, for example, linear peptides that may adopt an α-helix conformation upon binding to bacteria [16–26]. There are peptides that form β-sheets through cysteine coupling and cysteine-constrained loop structures [27–29]. However, there are also antimicrobial peptides that do not have such ordered structures but are characterized by an overrepresentation of certain amino acids [14].

Considering the role of the secondary structure, the amphiphilic nature of peptides, and the composition of bacterial membranes, it was thought that the function of antimicrobial peptides involves direct binding to the lipid bilayer and that interaction with bacterial membranes is a prerequisite for the function of antimicrobial peptides. However, the mechanism of the action of antimicrobial peptides on bacteria is complex [14,30–32]. On this basis, we distinguish between membrane-disrupting and non-membrane-disrupting peptides [14,32]. In several cases, heparin-binding motifs [33], as well as peptide sequences of endogenous proteins [34–36], matrix proteins [37], growth factors [38], and histidine-rich glycoproteins [39–47] have been shown to have antimicrobial activity, and are thus classical peptides and proteins of innate immunity. It is worth noting that there are other ways to prevent bacteria growth on surfaces, like polymeric coating or metal ions, on the surface [48,49]. These competitive systems are also important because the use of human-type peptides carries the risk of resistance.

These peptides, like other compounds [50–52] with antimicrobial activity, often have significant SOD activity. Based on these observations, the possible antimicrobial effects of the C-terminal heparin-binding domain of CuZnSOD were also investigated [15]. The results show that the CuZnSOD peptide segment has antimicrobial activity, which also means that peptides of human proteins may help to develop antimicrobial peptides based on endogenous peptides.

One direction of our research is the characterization of peptides modeling the CuZnSOD enzyme and the determination of their biological activity [53], and these results may contribute to the development of novel antimicrobial peptides.

The two binding sites of the CuZnSOD enzyme are the Zn(II)-binding HVGD sequence (fragments 80–83) and the Cu(II)-binding HVH sequence (fragments 46–48), and the two metal ions are connected by the imidazolatee ring of His63 [5]. In order to mimic the two binding sites, we synthesized 10-, 15-, and 16-membered peptides containing two or three binding sites in an environment corresponding to the native enzyme: Ac-FHVHEGPHFN-NH_2 (L^1(10)), Ac-FHVHAGPHFNGGHVG-NH_2 (L^2(15)), and Ac-FHVHEGPHFNGGHVGD-NH_2 (L^3(16)). pH-potentiometric, UV-Vis-, and CD-spectroscopy studies of the Cu(II), Zn(II), and Cu(II)-Zn(II) mixed complexes of these peptides were performed, and the SOD activity of the complexes was tested.

2. Experimental

2.1. Chemicals

To synthesize the oligopeptides (Ac-FHVHEGPHFN-NH_2 (L^1(10)), Ac-FHVHAGPH FNGGHVG-NH_2 (L^2(15)), and Ac-FHVHEGPHFNGGHVGD-NH_2 (L^3(16))), solid phase peptide synthesis was performed using a microwave-assisted Liberty 1 Peptide Synthesizer (CEM, Matthews, NC, USA). Fmoc/tBtu technique and TBTU/HOBt/DIPEA activation strategy were used. A detailed description of the procedure has already been published in our previous papers [54–56]. The chemicals and solvents used for synthetic purposes were obtained from commercial sources in the highest available purity and used without further purification. The Rink Amide AM resin (substitution: 0.70 mmole/eq), all of

the N-fluorenylmethoxycarbonyl (Fmoc)-protected amino acids (Fmoc-Ala-OH, Fmoc-Asp(O*t*Bu)-OH (O*t*Bu: 5-tert-butyl), Fmoc-Phe-OH, Fmoc-Gly-OH, Fmoc-His(Trt)-OH (TrT: trityl), Fmoc-Val-OH Fmoc-Glu(O*t*Bu)-OH), and 2-(1-H-benzotriazole-1-yl)-1,1,3,3-tetramethyluronium tetrafluoroborate (TBTU) are Novabiochem (Switzerland) products. N-hydroxybenzotriazole (HOBt·H_2O), N-methylpyrrolidone (NMP), triisopropylsilane (TIS), 2,2′-(ethylenedioxy)diethanethiol (DODT), and 2-methyl-2-butanol were purchased from Sigma-Aldrich Co., St. Louis, MO, USA, while N,N-diisopropyl-ethylamine (DIPEA) and trifluoroacetic acid (TFA) were Merck Millipore Co. products, Burlington, MA, USA. Peptide-synthesis grade N,N-dimethylformamide (DMF) and acetic anhydride (Ac_2O) were bought from VWR International, while piperidine, dichloromethane (DCM), diethyl ether (Et_2O), acetic acid (96%) (AcOH), and acetonitrile (ACN) were from Molar Chemicals Ltd., Halasztelek, Hungary. The peptide was characterized by ESI-MS, and the data is collected in Table A1.

The concentrations of the peptide stock solutions were determined by pH-potentiometric titrations. The stock solutions of copper(II) chloride, nickel(II) chloride, and zinc(II) chloride were prepared from analytical grade reagents, and their concentrations were checked gravimetrically via the precipitation of oxinate.

2.2. High-Performance Liquid Chromatography

The purity of the synthesized product was checked by analytical RP-HPLC monitoring the absorbance at 222 nm using a Jasco instrument equipped with a Jasco MD-2010 plus multiwavelength detector. The elution method was set as 0% of solvent B at 0 min, which begins to increase after 1 min up to 12% in 14 min and decreases to 0% again after 9 min. The gradient profile was achieved using solvent A (0.1 v/v% TFA in water) and solvent B (0.1 v/v% TFA in MeCN) at a flow rate of 1.0 mL/min. The solid phase was a Teknokroma Europa Protein C18 chromatographic column (250 mm × 4.6 mm, 300 Å pore size, 5 µm particle size) in the separation procedure.

The peptides were separated by RP-HPLC semipreparative Teknokroma Europa Protein 300 C18 column (250 mm × 10 mm, 5 µm). Reverse phase HPLC was performed on a Jasco instrument equipped with a Jasco UV-2077 Plus 4-λ Intelligent UV/Vis detector. The flow rate of 3 mL·min^{-1} was maintained. The elution of peptides was monitored by UV absorbance at 222 nm. The gradient elution mentioned above was used in this system.

2.3. Potentiometric Measurements

In total, 3 mL aliquots of the ligands and 0.2 M carbonate-free potassium hydroxide solution titrant were used for pH-potentiometric measurements. In order to avoid side reactions with carbon dioxide and/or oxygen, the headspace over the sample was purged with argon gas during titration, in which the concentration of the ligand was ca. 2 mM. KCl in 0.2 M concentration was used as a background electrolyte. Interaction with metal ions was studied in samples containing copper(II) chloride, zinc(II) chloride, or nickel(II) chloride at 1:3, 1:1, and 2:1 metal-to-ligand ratios. All pH-potentiometric measurements were carried out at 298 K, and an IKA Topolino magnetic stirrer, IKA, Wilmington, NC, USA was used to stir the samples. To perform the titrations, a MOL-ACS microburette was used, controlled by a computer, and a Molspin pH-meter equipped with a Metrohm 6.0234.100 combination glass electrode detected the pH data which were converted into hydrogen ion concentrations according to the method described by Irving et al. [57] SUPERQUAD [58] and PSEQUAD [59] computational programs enabled the calculation of the protonation constants of the ligands and the stability constants ($\log\beta_{pqr}$ for $M_pH_qL_r$species) of the metal complexes. Equations (1) and (2) define the equilibrium constants:

$$pM + qH + rL \rightleftharpoons MpHqLr \quad (1)$$

$$\beta_{pqr} = \frac{[M_pH_qL_r]}{[M]^p \cdot [H]^q \cdot [L]^r} \quad (2)$$

2.4. Spectroscopic Studies

UV-visible absorption spectra were recorded under the same conditions as the pH-potentiometric measurements in a 2.5 mL solution at different pH values. A Perkin Elmer Lambda 25 spectrophotometer, PerkinElmer, Waltham,MA, USA was used, and the absorption spectra were recorded in the 250–1100 nm wavelength range for copper(II) and nickel(II) containing systems at a metal-to-ligand ratio of 1:2 to 2:1 in a 1.00 cm cuvette.

The circular dichroism (CD) spectroscopic measurements were carried out on a Jasco-810 spectropolarimeter using the same ligand and metal concentrations and ratios as described above. CD-spectra were recorded in silica cells of 1.00 cm path length in the 280–800 nm range and 0.10 cm between 220 and 300 nm.

2.5. Superoxide Dismutase Activity

The superoxide dismutase (SOD) activity of the complexes was determined by the indirect method of NBT reduction [60]. The superoxide anion was generated in situ by the xanthine/xanthine oxidase reaction and detected spectrophotometrically by monitoring the reduction of NBT at 560 nm. The tests were carried out in phosphate buffer (50 mM) at pH 6.8 containing NBT (4.5×10^{-2} mM) and xanthine (0.2 mM). The reaction was initiated by adding an appropriate amount of xanthine oxidase to generate a change in absorbance around ΔA560 = 0.020–0.025 min^{-1}. The NBT reduction rate was measured in the presence and the absence of the investigated system ([Cu(II)]tot = 0–2.1 μM) for 480 s. For the greater reproducibility of the measured data, we started each measurement by monitoring a blank sample (without any Cu(II) complex) for 3–4 min, then the Cu(II) complex—prepared in phosphate buffer—was added to the sample. The change in the absorbance was monitored for another 4 min. The corresponding rates were obtained by fitting the experimental data to a straight line. The SOD activity was then expressed by the IC_{50} values (the concentration that causes 50% inhibition of NBT reduction). For calculating the inhibition, the following equation is used:

$$inhibition\% = \frac{\left(\frac{\Delta A}{time}\right)^{blank} - \left(\frac{\Delta A}{time}\right)^{complex}}{\left(\frac{\Delta A}{time}\right)^{blank}} \times 100 \quad (3)$$

where $\left(\frac{\Delta A}{time}\right)^{blank}$ is the change in absorbance per minute at 560 nm in the absence of complex and $\left(\frac{\Delta A}{time}\right)^{complex}$ is the change in absorbance per minute in the presence of X μM of the complex. Then, the IC_{50} values can be obtained from inhibition vs. complex concentration plots as follows: complex concentration, X [μM] = IC_{50} values where inhibition % = 50. The data can be fitted by using equation [61]:

$$Y(inhibition) = \frac{A \times c_{Cu(II)-complex}}{B + A \times c_{Cu(II)-complex}} \quad (4)$$

where Y stands for the inhibition, and A and B are parameters. The IC_{50} values were converted to relative activity that was calculated based on the following equation [53]:

$$relative\ activity = \frac{IC_{50}(CuZnSOD)}{IC_{50}(complex)} \times 100 \quad (5)$$

and then converted to the k_{cat} value as follows [62]:

$$k_{cat=}\frac{k_{NBT} \times [NBT]}{IC_{50}} \quad (6)$$

3. Results and Discussion

3.1. Protonation Equilibria of the Peptides

The deprotonation constants of the studied peptides were determined by means of pH-potentiometric titrations, and the data are collected in Table 1. All three peptides contain three or four histidine residues, while the deca- and hexadeca-peptides contain an aspartate and/or a glutamate side chain in addition to imidazole groups. The structural formulae of the studied peptides are shown in Scheme 1.

Table 1. The deprotonation constants of peptides completed with literature data (I = 0.2 M KCl, T = 298 K, standard deviations are in parentheses).

	pK(Asp)$_1$	pK(Asp)$_2$	pK(Glu)	pK (His)$_1$	pK(His)$_2$	pK(His)$_3$	pK(His)$_4$
L^1(10)	–	–	4.15 (3)	5.97 (2)	6.32 (1)	–	7.62 (7)
L^2(15)	–	–	–	5.43 (1)	6.12 (1)	6.47 (1)	6.83 (2)
L^3(16)	3.49 (1)		4.27 (1)	5.60 (1)	6.36 (1)	6.53 (1)	7.85 (3)
Ac-HADHAH-NH_2 [63]	2.83	–	–	5.90	–	6.48	7.11
Ac-HDHAHDH-NH_2 [63]	2.96	3.72	–	5.75	6.38	6.66	7.17

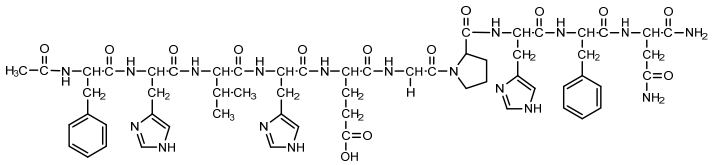

L¹(10) = Ac-FHVHEGPHFN-NH₂

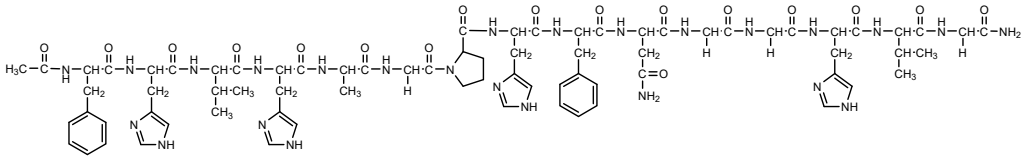

L²(15) = Ac-FHVHAGPHFNGGHVG-NH₂

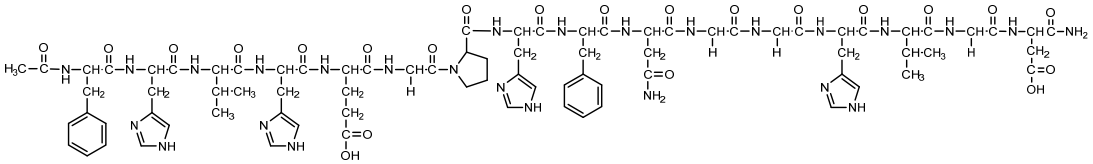

L³(16) = Ac-FHVHEGPHFNGGHVGD-NH₂

Scheme 1. Structural formulae of the studied peptides.

The carboxyl groups in the side chains of aspartic acid and glutamic acid are deprotonated in the acid pH range, and the smallest pK value belongs to the carboxyl group of aspartic acid residue. Upon increasing the pH, the deprotonation of the imidazolium groups in the side chain of histidines occurs in overlapping steps, as indicated by the small differences in pK(His) values, so that the pK values cannot be assigned to the different imidazolium groups. However, a comparison of the pK values of L^1(10) with those of L^2(15) and L^3(16) suggests that deprotonation of the C-terminal histidine (HVG(D) sequence) of the L^2(15) and L^3(16) peptides occurs around pH 6.5.

3.2. Copper(II) Complexes of the Peptides

The stoichiometry and the stability constants of the copper(II) complexes were obtained from the computer evaluation of titration curves recorded at different metal ion-to-ligand ratios. The stability constants and the derived constants are collected in Table 2. (The complexes of different ligands with the same stoichiometry have different charges; therefore, the charges are not shown.)

Table 2. Stability constants (log β) of complexes formed in the different Cu(II)-multihistidine peptide systems (T = 298 K, I = 0.2 M KCl).

	L^1(10)	**L^2(15)**	**L^3(16)**	**Ac-HADHAH-NH_2 [63]**	**Ac-HDHAHDH-NH_2 [63]**
$[CuH_3L]$	–	–	–	–	25.10
$[CuH_2L]$	–	19.21 (2)	21.18 (3)	–	–
[CuHL]	14.15 (2)	14.44 (2)	16.04 (7)	13.64	16.54
[CuL]	9.04 (2)	9.29 (2)	10.74 (6)	8.65	10.95
$[CuH_{-1}L]$	1.34 (12)	2.10 (7)	2.97 (12)	–	–
$[CuH_{-2}L]$	−6.56 (12)	–	–	−6.20	−4.36
$[CuH_{-3}L]$	−15.58 (9)	−12.42 (18)	−13.55 (9)	−15.70	−14.61
$[Cu_2L]$	–	12.18 (8)	–	–	–
$[Cu_2H_{-1}L]$	–	–	8.92 (12)	–	–
$[Cu_2H_{-2}L]$	–	0.64 (3)	–	−1.02	3.26
$[Cu_2H_{-3}L]$	–	–	−5.22 (43)	−7.54	–
$[Cu_2H_{-4}L]$	–	–	–	−14.64	−12.16
$[Cu_2H_{-5}L]$	–	–	−21.32 (33)	−23.64	−22.59
$[Cu_2H_{-6}L]$	–	−28.39 (12)	−30.45 (26)	−34.54	−33.84
log$K$(Cu(II) + 2N_{Im})	6.53	5.91	6.80	6.53	–
log$K$(Cu(II) + 3N_{Im})	9.04	7.61	8.19	8.65	9.37
log$K$(Cu(II) + 4N_{Im})	–	9.29	10.74	–	10.95
pK(Im)	5.11	4.77; 5.15	5.14; 5.30	4.99	4.28; 5.59
pK(amide)$_1$	7.70	7.19	7.77	7.42 (av.)	7.65 (av.)
pK(amide)$_2$	7.90	7.26 (av.)	8.26 (av.)		
pK(amide)$_3$	9.02			9.50	10.25

In the case of the 15-membered peptide, precipitation was observed in the pH range between 7 and 9, even in equimolar solution and in the presence of excess metal ions, so that the stability constants of the complexes can only be calculated with larger standard deviations.

For the studied peptides, the $[CuH_xL]$ species (x = 0, 1, 2) correspond to the two, three, or four imidazole coordinated monocomplexes, while the other histidine imidazole groups (in the case of x = 1, 2) are protonated.

A direct comparison between the stability constants of imidazole-coordinated species is not feasible. Therefore, derived equilibrium constants can be calculated for the complexes containing two, three, and four imidazole nitrogen atoms in the coordination sphere:

$$M + H_xL \rightleftharpoons MH_xL \quad (7)$$

$$\log K(M + z(N_{Im})) = \log \beta(MH_xL) - \log \beta(H_xL) \quad (8)$$

where x is the number of the non-coordinated histidine groups. These equilibrium constants are shown in Table 2 (log K(M + z(N_{Im})).

The stability of the two, three, and four imidazole coordinated complexes is generally close to each other for both the peptides currently studied and the previously studied 3 and 4 histidine-containing multihistidine peptides [53,63], but the presence of one or two carboxylate groups in side chains contributes to the stability of the complex. Comparing the log$K$(Cu(II) + 3Im) values of peptides to that obtained for the L^1(10) ligand containing two phenylalanyl side chains in addition to the glutamic carboxylate group, an extra stabilizing effect can be supposed to be due to the stacking effect between the metal ion and aromatic ring rings Thus, the stability of the three imidazole coordinated complexes increases in the order

$$L^2(15) < L^3(16) < \text{Ac-HADHAH-NH}_2 < L^1(10) < \text{Ac-HDHAHDH-NH}_2,$$

whereas the stability of the four imidazole coordinated complexes increases in the order

$$L^2(15) < L^3(16) < \text{Ac-HDHAHDH-NH}_2$$

This order also shows that the formation of macrochelate structures by coordinating histidines that are close to each other (with one or two amino acids between them) is slightly more favorable for complex formation than peptides containing histidines in a more distal position. This is consistent with previous observations [64]. Figure 1 shows the distribution curves of the complexes formed in the equimolar system of the three peptides. In the pH range indicated by the dashed line (b), a precipitate was present in the solution. These pH-potentiometric data were not taken into account for the evaluation. In all cases, the stabile three and/or four imidazole coordinated complexes are predominant species in the slightly acidic and physiological pH range (Figure 1).

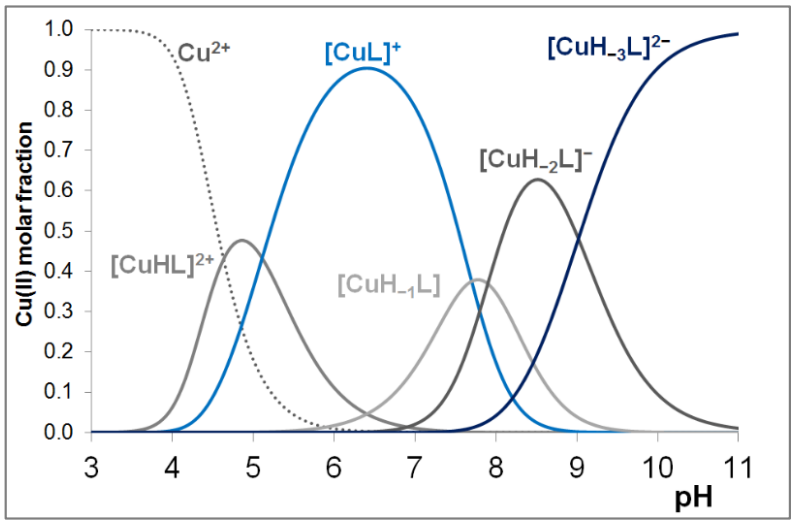

(**a**)

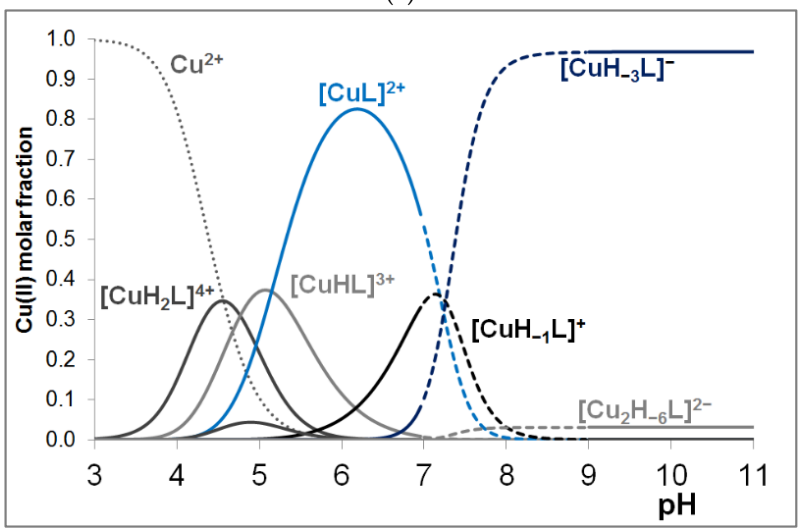

(**b**)

Figure 1. *Cont.*

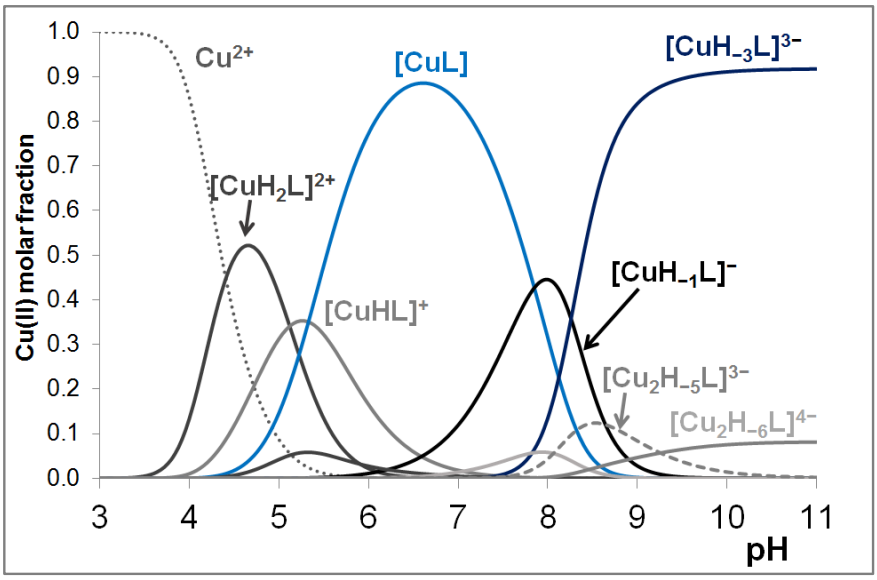

(**c**)

Figure 1. Distribution curves of the complexes formed in equimolar solution of Cu(II)-L^1(10) (**a**), Cu(II)-L^2(15) (**b**) and Cu(II)-L^3(16) (**c**) systems ($c_L = c_{Cu(II)}$ = 1 mM).

However, similarly to the previously studied multihistidine peptides, the formation of imidazole-coordinated complexes cannot prevent the deprotonation and coordination of amide nitrogens of the peptide backbone. In all cases, the imidazole group of the histidine residue serves as the anchoring group to induce the deprotonation and coordination of the preceding peptide amide nitrogens. Upon increasing the pH, the deprotonation and coordination of one (two) and three amide groups take place, leading to the formation of $[CuH_{-1}L]$, $[CuH_{-2}L]$, and $[CuH_{-3}L]$ complexes. For the pentadeca- and hexadecapeptide, the deprotonation of second- and third-amide nitrogen occurs in cooperative reactions. The stepwise deprotonation constants of these processes can be found in the last four rows of Table 2.

The reported p*K*(amide) values show that stabile [CuL] complexes of peptides mimicking the binding sites of CuZnSOD enzymes shift the deprotonation of amide groups into the alkaline pH range, and the deprotonation of the first peptide nitrogen occurs at higher pH than that reported for terminally protected single histidine-containing peptides (e.g., Ac-GNGAHKPG-NH_2 p*K*(amide) values are 6.68 (5.38) and 7.18) [65]. These effects are well reflected by the distribution curves of the copper(II) complexes (Figure 1).

The presence of three or four histidines in the peptide sequence offers more than one binding site in the molecule. As the data collected in Table 2 shows, dinuclear complexes are formed when copper(II) ion is applied in excess. In these species, similarly to the mononuclear complexes, the imidazole and 1–3 deprotonated amide nitrogen are coordinated to copper(II) ion (see Scheme 2b).

Different spectroscopic methods were used to establish the coordination modes of the complexes. The visible spectral parameters of the copper(II) complexes are included in Table 3. Figure 2 represents the distribution curves of the complexes formed in the copper(II)–L^3(16) = 2:1 system together with the change of the absorption maxima. By increasing pH, a blue shift of the absorption maxima is observed in agreement with the changes in the coordination sphere around the metal ion. The wavelengths of the measured absorption maxima are in good agreement with those obtained for other multihistidine peptides with the same coordination mode.

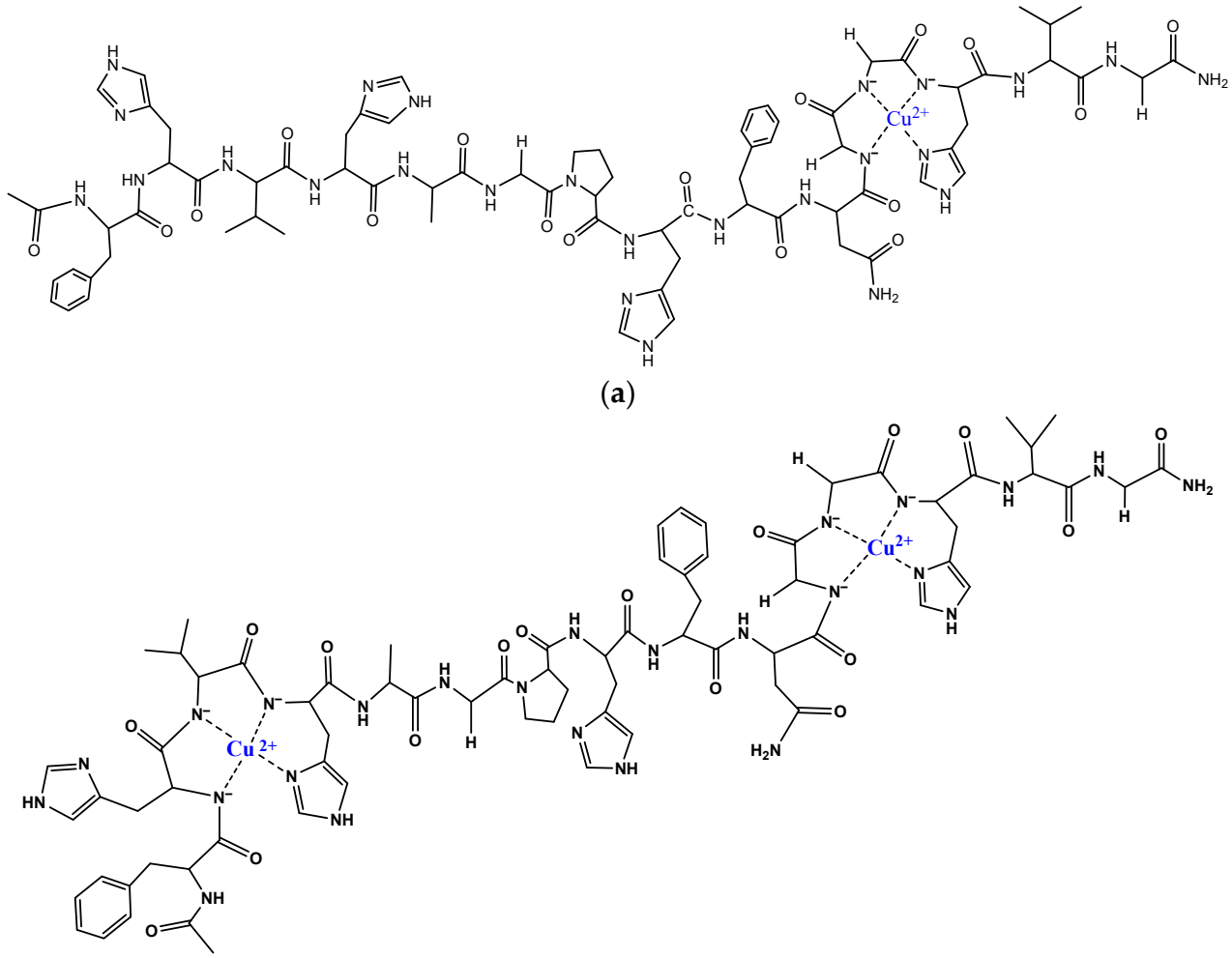

Scheme 2. Schematic structure of $[CuH_{-3}L]^{-}$ (**a**) and $[Cu_2LH_{-6}]^{2-}$ (**b**) of L^2(15) peptide.

Table 3. Visible spectral parameters of the copper(II) complexes of multihistidine peptides (w = wide).

Species	Binding Mode	λ_{max} (nm) (ε (M^{-1} cm^{-1}))				
		L^1(10)	L^2(15)	L^3(16)	Ac-HADHAH-NH_2 [63]	Ac-HDHAHDH-NH_2 [63]
[CuL]	[3 × Im] or [4 × Im]	624 (52) w	615 (97) w	600 (108) w	615 (85)	605 (60)
$[CuH_{-3}L]$	[N^-, N^-, N^-, Im]	530 (102)	536 (166) w	540 (147) w	532 (132)	538 (103)
$[Cu_2H_{-6}L]$	2 × [N^-, N^-, N^-, Im]	–	545 (191) w	537 (163) w	–	–

These data support the formation of 3 or 4 imidazole-coordinated complexes (CuL) in the physiological pH range, while 4N-coordinated species form in strong alkali medium($CuH_{-3}L$, $Cu_2H_{-6}L$). Both in equimolar solution and in Cu(II):L = 2:1 solution, an intense absorption maximum appears at around 530−540 nm in alkaline pH, confirming that the coordination mode of the metal ions in the mononuclear and dinuclear complexes is [N^-, N^-, N^-, Im]. Based on the empirical formula [66], the calculated value of λ_{max} for the [N^-, N^-, N^-, Im] coordination environment is expected to be 522 nm, which slightly differs from the measured values. However, we need to note that the absorption bands are quite broad, indicating the presence of coordination isomers.

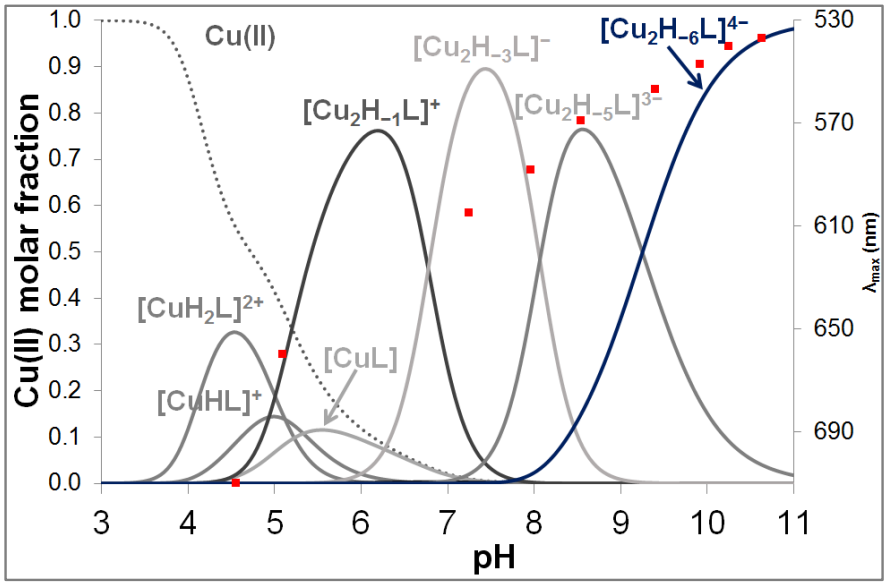

Figure 2. Metal ion speciation of the copper(II)-L^3(16) system at 2:1 metal-to-ligand ratio (c_L = 1 mM) are plotted together with the change of absorption maxima (■).

Circular dichroism spectroscopic studies were carried out to confirm the assumed coordination modes of the complexes and to estimate the ratio of coordination isomers. The CD parameters of the copper(II) species are included in Table A2 in the Appendix A.

No measurable CD activity was observed in slightly acidic media, supporting the exclusive coordination of the imidazole side chains in the [CuH_xL] and [CuL] complexes (x = 1, 2). Above pH 8, an intense positive Cotton effect is observed at around 250–300 nm, which is characteristic of the $N^- \rightarrow Cu^{2+}$ charge transfer band. The deprotonation of the amide nitrogen atoms results in intense bands in the visible region of the spectra around 650 (negative Cotton effect) and 520 nm (positive Cotton effect). This is well presented in Figure A1 in the Appendix A, where CD spectra of the Cu(II)–L^3(16) = 1:1 system are shown as a function of pH. Figures 3 and A2 (in the Appendix A) are used to compare the spectra recorded at 1:1 and 2:1 copper(II)-to-ligand ratios.

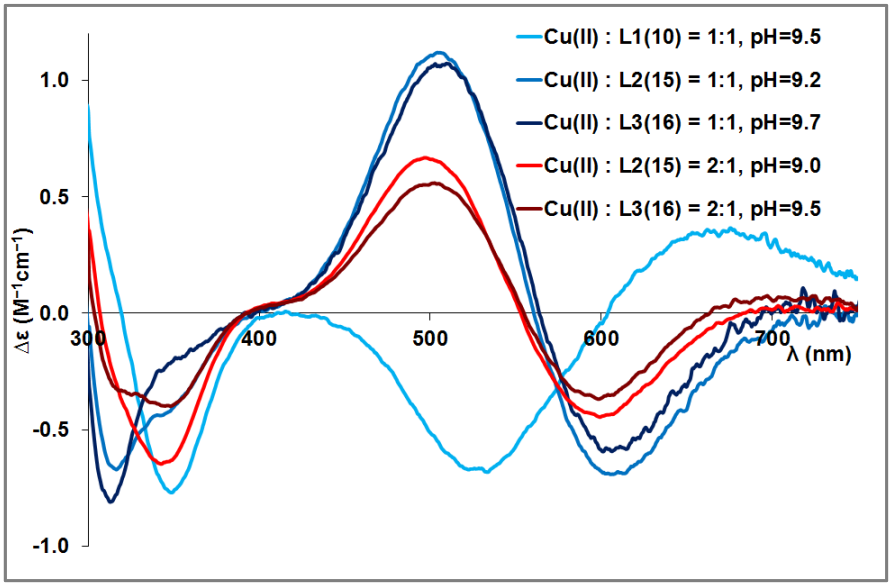

Figure 3. CD spectra of the copper(II) complexes of L^1(10), L^2(15) and L^3(16) around pH 9–9.7 at Cu(II)-L = 1:1 and 2:1 ratios (c_L = 0.7 mM).

It is obvious that CD spectra of copper(II)-L^2(15) and copper(II)-L^3(16) systems are similar around pH 8.0 and 9.5, and the metal ion-to-ligand ratio has no significant effect on the shape of the CD curves (Figure 3). The same similarity of the spectra can be observed at pH 11 in equimolar solutions of copper(II)-L^2(15) and copper(II)-L^3(16) and in the presence of copper(II) excess (Figure 3). The shape of CD spectra registered in copper(II)-L^1(10) systems is, however, different from those of longer peptides at all studied pH. These observations can be explained by the fact that L^2(15) and L^3(16) ligands offer more potential binding sites for copper(II) ions, and the coordination of copper(II) ions to different histidine-containing sequences in the molecule results in different types of CD spectra. The ligands L^2(15) and L^3(16) contain two preferred binding sites, the N-terminal -HVH- sequence and the C-terminal -GGH- sequence. The fourth histidine is in the amino acid environment, -GPHFN-, which is less favorable for metal binding because of the presence of a proline in the vicinity of histidine. In contrast, in the L^1(10) peptide, only the N-terminal -HVH- binding site may be the primary binding site for the metal ion. The comparison of the CD spectra of the copper(II) complexes of three oligopeptides with those of the other previously studied peptides helps to estimate the main copper(II) binding site of the ligands.

The positive Cotton effect observed at around 650 nm corresponds to the copper(II) binding site of the -HXH- sequence [63], while the band at around 500 nm can be observed when the metal ion coordinates to the -GXH- motif [65,67]. As a consequence, copper(II) ion binds mainly to the C-terminal -(NGG)HVGD- binding site in the case of 15- and 16-membered peptides. Since this part is missing from the L^1(10) peptide, the -FHVH- part could serve as a main binding site. This is consistent with the fact that the CD spectrum of the copper(II)-L^1(10) system is different from those of the other two peptides, and its shape is similar to that of the Ac-SarHAH-NH_2 peptide [63]. An estimate of the ratio of the binding sites can be obtained by the superposition of two peptides modeling (Ac-SarHAH-NH_2 [63] and Ac-PHAAA-NH_2 [68]) the two binding sites in the appropriate ratio. Based on this, the ratio of the binding of copper(II) ion to the -FHVH- and -GPHFN- binding sites is about 60%:40% for the L^1(10) peptide (Figure 4a). Likewise, the ratio of copper(II) ions coordinated to different metal binding sites of L^2(15) and L^3(16) can be estimated by the superposition of the CD spectra of Cu(II) complexes of model peptides (Figure 4b, Figure A3a in the Appendix A).

These calculations show that in equimolar solutions and alkaline media, the majority of the Cu(II) coordinates to the -GGH- motif (Scheme 2a). When the metal ion is applied in two folds of excess, copper(II) ion is effectively bound to the two main binding sites, -HVH- and -GGH- sequences (Figure A3b, Scheme 2b); however, the involvement of the internal histidyl residue cannot be ruled out.

Since both L^2(15) and L^3(16) ligands have at least three potential metal ion binding sites, both ligands can bind more than two metal ions. This is illustrated in Figure A4 (in the Appendix A), where the CD spectra are depicted at different copper(II) ion-L^3(16) ratios. This reflects the difference between the curve recorded at 1:1, 2:1, and 3:1 metal ion-to-ligand ratios. In equimolar solutions, an intense positive Cotton effect is observed at around 500 nm, characteristic of the -GGH- sequence, indicating that copper(II) is predominantly bound by the C-terminal imidazole nitrogen in the mononuclear complexes. At a 2:1 metal ion-to-ligand ratio, a new positive band appears at around 650 nm, suggesting that one metal ion is coordinated by the N-terminal histidyl moiety while the other copper(II) is bound by the C-terminal part of the molecule.

At threefold metal ion excess, the ligand is able to bind three copper(II) ions: the negative Cotton effect at around 520 nm is characteristic of the [Im, N^-, N^-, N^-] coordination mode, supporting that not only the N- and C-terminal imidazole nitrogens but also the internal histidyl residue serves as binding sites for metal ion coordination. In conclusion, the formation of trinuclear complexes is also possible in the strongly alkaline range, but pH-potentiometric measurements have not been performed to calculate their stability constants

since this ratio is not relevant for biological systems, where the metal ion-to-protein ratio is much lower than 1:1.

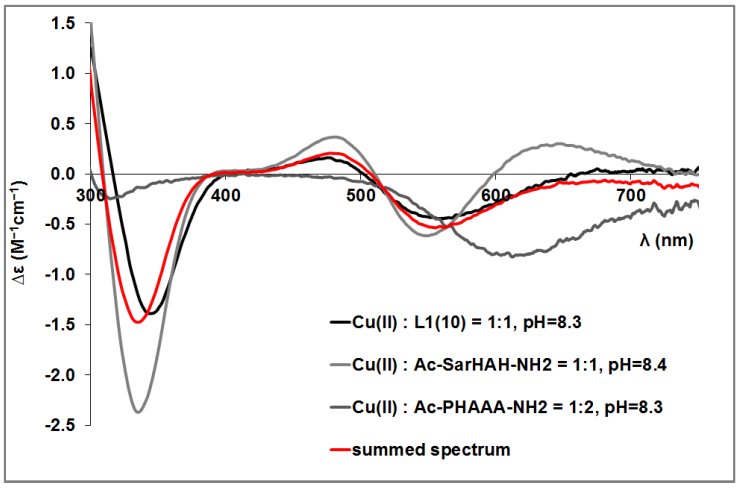

(**a**)

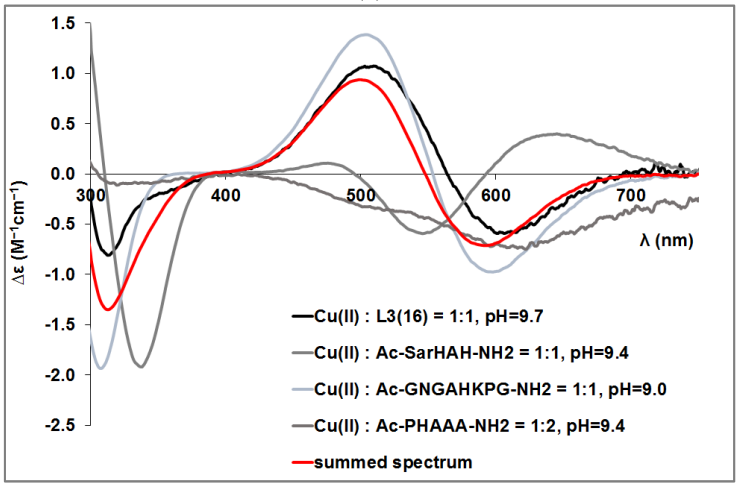

(**b**)

Figure 4. (**a**) CD spectra of Cu(II)-L1(10) (black), Cu(II)-Ac-SarHAH-NH_2, and Cu(II)-Ac-PHAAA-NH_2 complexes and spectra obtained by summing the CD spectra of Cu(II)-Ac-SarHAH-NH_2 and Cu(II)-Ac-PHAAA-NH_2 in 60%:40% ratio (red) at pH ~8.3; (**b**) CD spectra of the Cu(II)-L^3(16) (black), Cu(II)-Ac-SarHAH-NH_2, Cu(II)-Ac-GNGAHKPG-NH_2 and Cu(II)-Ac-PHAAA-NH_2 complexes and spectra obtained by summing the CD spectra of Cu(II)-Ac-SarHAH-NH_2, Cu(II)-Ac-GNGAHKPG-NH_2 and Cu(II)-Ac-PHAAA-NH_2 in 70%:25%:5% ratio (red) at pH ~9.3.

3.3. Zinc(II) Complexes of the Peptides

The stability constants of the mononuclear zinc(II) complexes of the studied peptides are collected in Table 4, while the distribution curves of the complexes formed in the equimolar solution of the three ligands are shown in Figure A5 in the Appendix A. In all cases, the [ZnL] stoichiometry corresponds to the coordination via histidyl side chains. A comparison of the log*K*(Zn-3Im) values of the imidazole-coordinated species reveals that the formation constants of complexes with ligands containing aspartic and/or glutamic acid residues are higher than those without negatively charged side chains. It suggests that the interaction of the carboxylate groups enhances the stability of the imidazole-N coordinated zinc(II) complexes. Interestingly, the log*K*(Zn-3Im) value obtained for the metal complex of the L^1(10) decapeptide containing only one negatively charged side chain is about 0.5 log unit higher than the formation constant calculated for the zinc(II)–L^3(16) complex with tridentate imidazole-N coordination mode. It indicates that the size of the molecules and the position of the aforementioned side chains have an effect on the

stability of the imidazole-coordinated complexes. This finding is in agreement with our previous results [63,64].

Table 4. Stability constants (log β) of complexes formed in the different Zn(II)-multihistidine peptide systems (T = 298 K, I = 0.2 M KCl).

	L^1(10)	L^2(15)	L^3(16)	Ac-HADHAH-NH_2 [63]	Ac-HDHAHDH-NH_2
$[ZnH_2L]$	–	17.38 (6)	18.51 (16)	–	18.18 (3)
[ZnHL]	11.54 (8)	12.08 (2)	13.22 (6)	10.91	12.80 (2)
[ZnL]	6.12 (2)	6.06 (2)	7.36 (4)	5.63	6.97 (2)
$[ZnH_{-1}L]$	−1.28 (6)	−0.95 (2)	−0.80 (7)	−2.40	−0.72 (3)
$[ZnH_{-2}L]$	−11.42 (8)	−10.60 (3)	−10.20 (7)	−11.23	–
log$K$(Zn(II) + $3N_{Im}$)	6.12	5.25	5.37	5.63	5.63
log$K$(Zn(II) + $4N_{Im}$)	–	6.06	7.36	–	6.97
log$K$($ZnL/ZnH_{-1}L$)	7.40	7.01	8.16	8.03	7.69
log$K$($ZnH_{-1}L/ZnH_{-2}L$)	10.14	8.65	9.40	8.83	–

In slightly alkaline solutions, $[ZnH_{-1}L]$ and $[ZnH_{-2}L]$ complexes are formed, which are not strong enough to hinder the hydrolysis of the metal ion, and precipitation occurs. This suggests that these species correspond to the formation of mixed hydroxido complexes, and metal ion-induced deprotonation of amide nitrogen atoms does not take place. The same phenomenon was observed in the previously studied Zn(II)–Ac-HXHZH-NH_2 systems [63].

3.4. Mixed Cu(II)/Zn(II) Complexes of the Peptides

The aforementioned results clearly reflect that in the parent copper(II) complexes of 15- and 16-membered peptides, the C-terminal histidine is the main binding site for copper(II) together with deprotonated amid nitrogen atoms, whereas for Zn(II), the main species in the physiological pH range are complexes with four imidazole coordinations. Since both metal ions bind to one of the specific peptide sequences in the native CuZnSOD enzyme, we found it worthwhile to investigate whether the binding site preference of the metal ions is altered when both metal ions are present. Thus, pH-potentiometric and spectroscopic studies of systems containing Cu(II), Zn(II) ions, and L^2(15) or L^3(16) peptides in equimolar concentrations were performed. In the case of the L^2(15) peptide, only the stability constant for one complex formed in the alkaline range could be determined because precipitation occurred in the pH range between 7 and 9. The mixed metal complexes of peptide L^3(16) could be analyzed below pH ~10 because in this case, precipitation occurred above pH 10. The precipitation redissolved only in a strongly basic solution. The stability constants of the formed mixed metal complexes are collected in Table 5.

Table 5. Stability constants (log β) of complexes formed in the different Cu,Zn(II)-L^2(15) and –L^3(16) peptide systems. (T = 298 K, I = 0.2 M KCl).

	L^2(15)	L^3(16)
$[CuZnH_{-1}L]$	–	6.6 (4)
$[CuZnH_{-2}L]$	–	0.11 (5)
$[CuZnH_{-3}L]$	–	−7.95 (7)
$[CuZnH_{-4}L]$	–	−17.15 (9)
$[CuZnH_{-5}L]$	−22.7 (5)	–

In the mixed metal complexes, the copper(II) ion coordinates with the $[(N^-)_x,Im]$ coordination mode, while the zinc(II) ion is coordinated via the N donor atom of imidazole rings. In the $[CuZnH_{-5}L]$ complex, deprotonation of one of the water molecules coordinating to Zn(II) is also assumed. Figure 5 shows the concentration distribution curves of equimolar mixed

Cu(II)-Zn(II) L systems (L = L^2(15) and L^3(16)), where the total molar fraction of Cu(II) and Zn(II) parent complexes and mixed metal complexes are plotted, respectively.

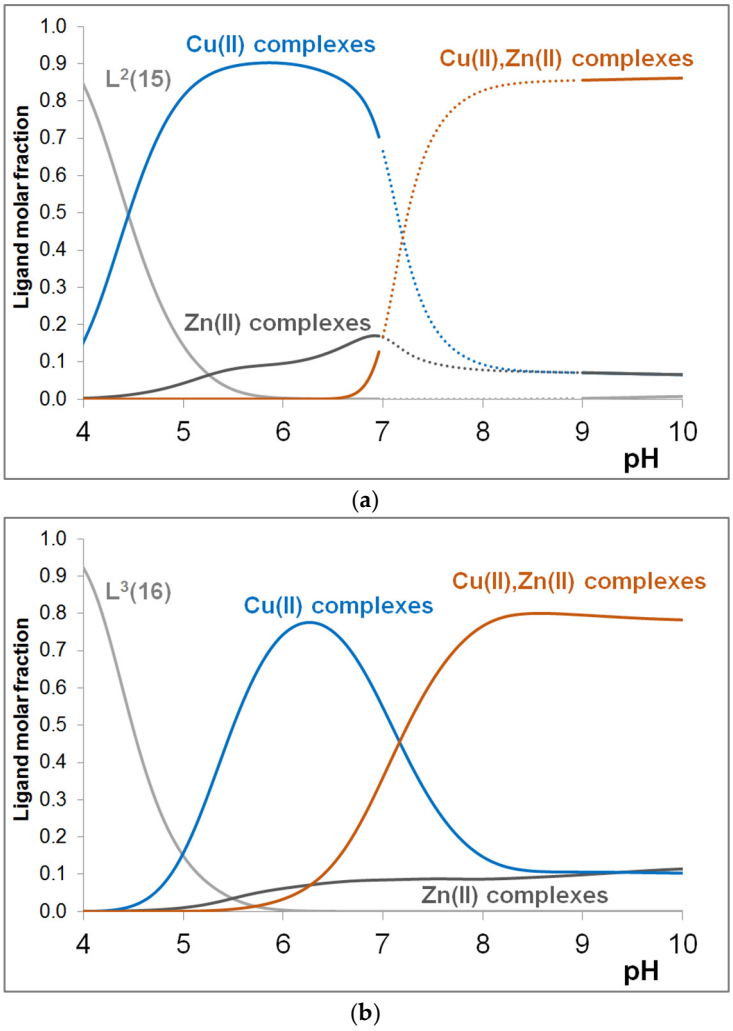

Figure 5. Distribution curves of complexes formed in the equimolar solution of Cu(II),Zn(II)-L^2(15) (**a**) and Cu(II),Zn(II)-L^3(16) (**b**) systems $c_L = c_M = 0.8$ mM. (The dotted line indicates the pH range where precipitation was formed).

Below pH 6, all the ligands mainly coordinate to copper(II) ion, whereas in the physiological and alkaline pH range, mixed metal complexes predominate. The formation of mixed metal complexes in the physiological and alkaline pH range can modify the distribution of metal ions between potential binding sites. CD spectroscopic studies have provided the opportunity to follow these processes. Figure 6 illustrates that in the slightly alkaline pH range, in the presence of Zn(II), the CD spectrum changes compared to the spectrum recorded in the equimolar solution of Cu(II), and the spectra of systems containing copper(II), zinc(II) and ligand in a 1:1:1 ratio are similar to those recorded at Cu(II)-L = 2:1 ratio (L = L^2(15) and L^3(16)). This confirms that the addition of Zn(II) results in a redistribution of Cu(II) among the potential binding sites and that Zn(II) binds at least partially to the C-terminal part of the peptides, corresponding to the Zn(II) binding site of CuZnSOD enzyme. A similar conclusion can be drawn from Figure A6 (in the Appendix), where the CD spectra of Cu(II)-Zn(II)-L^3(16) are plotted in the function of Cu(II)-Zn(II) ratio.

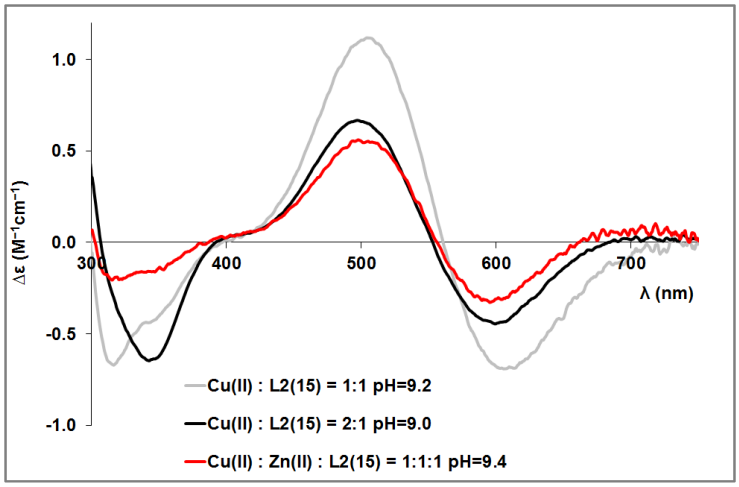

(**a**)

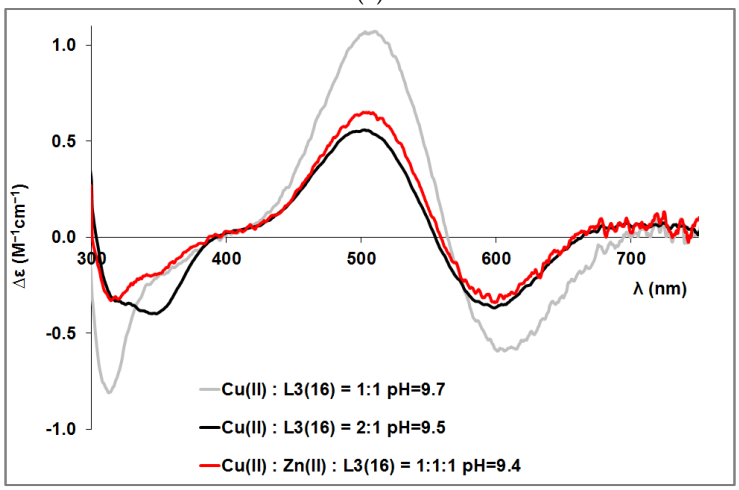

(**b**)

Figure 6. CD spectra registered in the Cu(II)-L^2(15) = 1:1 (gray), Cu(II)-L^2(15) = 2:1 (black) and Cu(II)-Zn(II)-L^2(15) = 1:1:1 (red) systems (c_L = 0.8 mM) (**a**) and in the Cu(II)-L^3(16) = 1:1 (gray), Cu(II)-L^3(16) = 2:1 (black) and Cu(II)-Zn(II)-L^3(16) = 1:1:1 (red) systems (**b**) (c_L = 0.9 mM).

3.5. Superoxide Dismutase Activity Measurements:

As a continuation of our work, we measured the SOD activity of the complexes of L^2(15) and L^3(16), and the SOD activity assay was also completed with the study of complexes of four histidine-containing heptapeptides (Ac-HDHAHDH-NH_2). The assays were performed in samples containing equimolar amounts of Cu(II) and peptide and Cu(II), Zn(II), and peptide (c_L = $c_{Cu(II)}$ = 2 μM and c_L = $c_{Cu(II)}$ = $c_{Zn(II)}$ = 2 μM), and the pH of the samples was adjusted to 6.8 with phosphate buffer ($c(PO_4^{3-})$ = 50 mM) as described in the experimental section. The inhibition curves recorded for Cu(II)-L^2(15) and Cu(II)-L^3(16) are illustrated in Figure 7. The IC_{50} values determined for all the systems studies are given in Table 6. In addition, data for previously studied multihistidine peptides and some other copper(II) and manganese(III) complexes are also included in the table. A better comparison is facilitated by the calculation of the relative activity, where the measured values are compared to the IC_{50} value of the SOD enzyme measured under the same conditions [53].

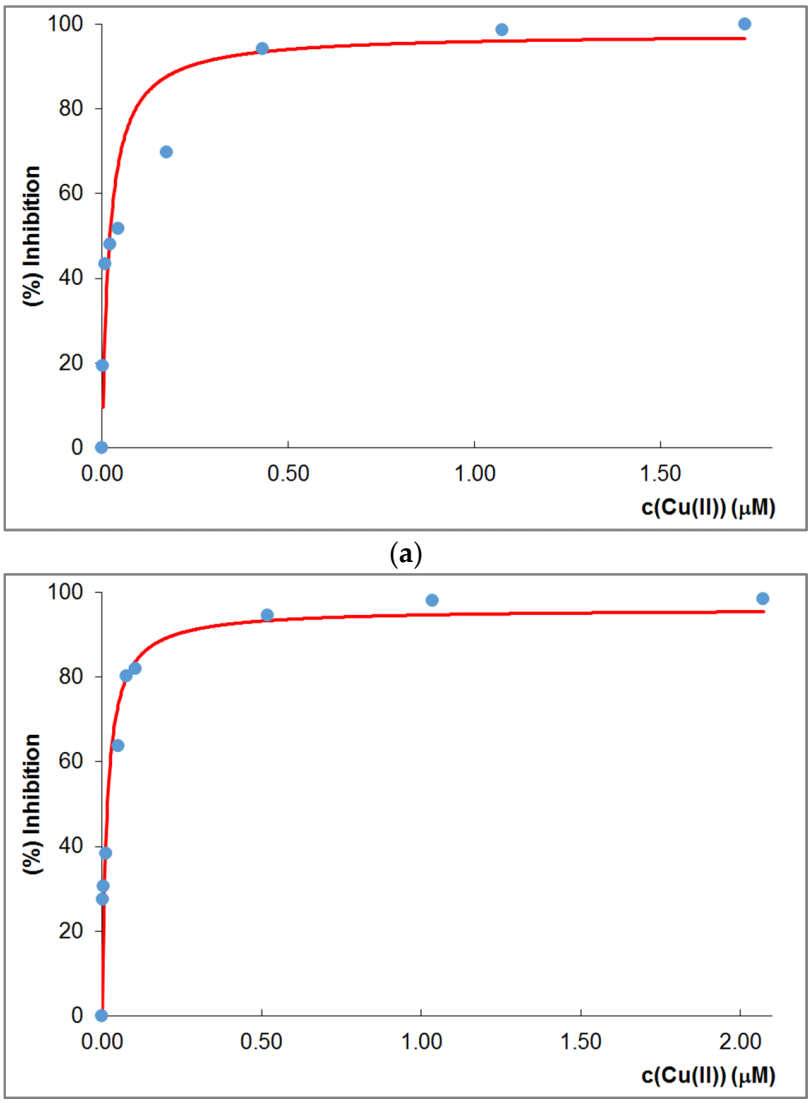

Figure 7. The inhibition of NBT-superoxide anion reaction with Cu(II)-L^2(15) (**a**) and Cu(II)-L^3(16) (**b**) complexes at pH 6.8 (measured points: marked by blue symbols; calculated points: marked by the continuous red lines based on Equation (5)).

Table 6. IC_{50} and relative activity values and the catalytic SOD activity of the complexes at pH = 6.8.

System	pH	IC_{50} (μM)	Relative Activity % [63]	$k_{cat}/10^6$ ($M^{-1}s^{-1}$)	Ref.
CuZnSOD	6.8	0.0030	100	914	[53]
CuZnSOD		0.010		430	[69]
Cu(II)-L^3(16)	6.8	0.017 ± 0.004	17.6	161	this work
Cu(II)-Zn(II)-L^3(16)	6.8	0.014 ± 0.002	21.4	196	this work
Cu(II)-L^2(15)	6.8	0.021 ± 0.007	14.3	131	this work
Cu(II)-Zn(II)-L^2(15)	6.8	0.019 ± 0.008	15.8	144	this work
Cu(II)-Ac-HDHAHDH-NH_2	6.8	0.020 ± 0.006	15.0	137	this work
Cu(II)-Ac-HAAHGH-NH_2	6.8	0.072	4.17		[53]
Cu(II)-Ac-HGGGHGH-NH_2	6.8	0.071	4.22		[53]
Cu(II)-PydiTyr		0.028		96.2	[70]
$[Mn(PI)_2](PF_6)(CH_3CN)$	7.0	0.87		6.6	[62]
$[Mn(III)Cl_4$ TE-2-PyP]		0.0065		400	[71]

The data reflect that the SOD activity of the copper(II) complexes of the studied 15- and 16-membered peptides is outstandingly good, and similarly, good IC_{50} values were obtained for the heptapeptide containing four histidines. However, practically the same activity values were also measured in the equimolar Cu(II)-Zn(II)-L^2(15) and Cu(II)-Zn(II)-L^3(16) systems. Although it was expected that the rearrangement of the binding of metal ions in the presence of Zn(II) would have an effect on SOD activity, the answer is given by the distribution curves calculated for the conditions of measurement. Figures A7 and A8 in the Appendix A show the distribution of Cu(II)-L^2(15), Cu(II)-L^3(16), and Cu(II)-Zn(II)-L^2(15), Cu(II)-Zn(II)-L^3(16), respectively, for the concentrations used in the SOD activity measurements. The figures clearly show that Cu(II) complexes (CuL) with only imidazole coordination dominated in the Cu(II)-L^2(15) and Cu(II)-L^3(16) systems under these conditions, while the proportion of Cu(II)-Zn(II) mixed complexes is much lower in Cu(II)-Zn-L (L = L^2(15) or L^3(16)) systems. Thus, the presence of zinc at pH 6.8 does not affect the SOD activity values. Although the relative SOD activity of the complexes studied is smaller than that of the native CuZnSOD enzyme, it is important to note that the complexes showed better performance in the degradation of superoxide anion than other SOD mimics. Thus, the incorporation of specific amino acid sequences mimicking the CuZnSOD enzyme increases the efficiency of model systems in the catalytic decomposition of superoxide anion.

4. Conclusions

The Cu(II), Zn(II), and Cu(II)-Zn(II) mixed complexes of 10-, 15-, and 16-membered model peptides containing both the copper(II) and zinc(II) binding sites of the CuZnSOD enzyme were investigated by pH potentiometry and spectroscopic methods, and these studies were completed by measurements of the SOD activity of Cu(II) and Cu(II)-Zn(II) mixed complexes at pH 6.8.

We have found that all the histidine imidazole rings can act as anchor groups for Cu(II). In the physiological pH range, the imidazole-coordinated complexes dominate, whereas deprotonation of amide nitrogens occurs in the alkaline pH range, and Cu(II) coordinates with the (N^-, N^-, N^-, Im) donor set. In the equimolar solution, the –(NGG)HVGD– sequence of the peptides, which mimics the Zn(II) binding site of the native enzyme, is the preferred binding site, as confirmed by UV-vis and CD spectroscopic studies. However, due to the presence of more histidine, the peptides can bind more than one Cu(II) ion, and thus, in solutions containing an excess of Cu(II) ions, we observed the formation of dinuclear complexes with Cu(II) binding to the –FHVH– and –(NGG)HVGD– sequences in nearly equimolar ratios.

In Cu(II)-Zn(II)-L (L = L^2(15) or L^3(16)) mixed systems, the presence of Cu(II)-Zn(II) complexes could only be detected in the alkaline range. The spectroscopic measurements, however, confirm that the addition of Zn(II) results in a redistribution of Cu(II) among the potential binding site, and Zn(II) binds at least partially to the C-terminal part of the peptides, corresponding to the Zn(II) binding site of CuZnSOD enzyme.

Cu(II) complexes of 15- and 16-membered peptides showed high SOD activity. However, the presence of Zn(II) did not affect the activity because at the concentrations used in the measurements at pH 6.8, the parent Cu(II) complexes predominate.

It can be concluded that the studied model peptides, which contain the amino acid sequence corresponding to the two binding sites of the SOD enzyme, bring us closer to mimicking the enzyme. However, the effect of the larger distance between the binding sites in the native enzyme and the conformation of the molecule is not validated in these peptides, so we will continue the research with molecules obtained by further modification of these peptides.

Author Contributions: Conceptualization, E.S. and K.V.; formal analysis, E.S., M.M., N.L. and K.V.; investigation, E.S., M.M. and N.L.; resources, K.V.; writing—original draft preparation, E.S. and K.V.; writing—review and editing, K.V.; visualization, K.V.; supervision, K.V.; funding acquisition, N.L. and K.V. All authors have read and agreed to the published version of the manuscript.

Funding: This research was funded by János Bolyai Research Scholarship of the Hungarian Academy of Sciences and the New National Excellence Program grant number ÚNKP-22-5.

Institutional Review Board Statement: Not applicable.

Informed Consent Statement: Not applicable.

Data Availability Statement: Data is contained within the article or Appendix A.

Conflicts of Interest: The authors declare no conflict of interest.

Abbreviations

Ac_2O	acetic anhydride
AcOH	acetic acid
ACN	acetonitrile
A, Ala	alanine, alanyl
CD	circular dichroism spectroscopy
DCM	dichloromethane
DIPEA	N,N-Diisopropylethylamine
DMF	N,N-Dimethylmethanamide
DODT	2,2′-(Ethylenedioxy)diethanethiol
D, Asp	aspartic acid, aspartyl
Et_2O	diethyl ether
E, Glu	glutamine, glutamyl
Fmoc	fluorenylmethyloxycarbonyl
F, Phe	phenylalanine, phenylalanyl
G, Gly	glycine, glycyl
H, His	histidine, histidinyl
HOBt	1H-Benzotriazol-1-ol
HPLC	High-Performance Liquid Chromatography
IC_{50}	the concentration that causes 50% inhibition of NBT reduction
M, mM, μM	$mol \cdot dm^{-3}$, $mmol \cdot dm^{-3}$, $\mu mol \cdot dm^{-3}$
NBT	nitro blue tetrazolium chloride
NMP	N-methyl-pyrrolidone
N, Asn	asparagine, asparaginyl
O*t*Bu	5-tert-Butyl
P, Pro	proline, prolyl
RP-HPLC	Reversed-Phase High-Performance Liquid Chromatography
SOD	superoxide dismutase
TBTU	2-(1H-Benzotriazole-1-yl)-1,1,3,3-tetramethyluronium tetrafluoroborate
TFA	trifluoroacetic acid
TIS	triisopropylsilane
Trt	trityl
UV-vis	UV-visible spectroscopy
V, Val	valine, valyl
[X]	equilibrium concentration of X
β_{pqr}	stability constants of $M_pH_qL_r$ species
$\left(\frac{\Delta A}{time}\right)^{blank}$	the change in absorbance per minute at 560 nm in the absence of complex
$\left(\frac{\Delta A}{time}\right)^{complex}$	the change in absorbance per minute in the presence of X μM of the complex

Appendix A

Table A1. Measured and calculated m/z values of $L^1(10)$, $L^2(15)$ and $L^3(16)$ peptides.

Species	Composition	*m*/*z* (Measured)	*m*/*z* (Calculated)
$L^1(10)$			
L^-			
H_2L^+	$C_{59}H_{77}N_{18}O_{14}^+$	1261.629	1261.586
$NaHL^+$	$C_{59}H_{76}N_{18}NaO_{14}^+$	1283.620	1283.568
KHL^+	$C_{59}H_{76}KN_{18}O_{14}^+$	1299.592	1299.542
Na_2L^+	$C_{59}H_{76}N_{18}Na_2O_{14}^+$	1305.599	1305.599
$L^2(15)$			
L			
HL^+	$C_{74}H_{100}N_{25}O_{17}^+$	1610.768	1610.772
H_2L^{2+}	$C_{74}H_{101}N_{25}O_{17}^{2+}$	805.888	805.890
H_3L^{3+}	$C_{74}H_{102}N_{25}O_{17}^{3+}$	537.595	537.596
$L^3(16)$			
L^{2-}			
H_3L^+	$C_{80}H_{107}N_{26}O_{22}^+$	1783.78	1783.8048
NaH_2L^+	$C_{80}H_{106}N_{26}NaO_{22}^+$	1805.77	1805.7867
KH_2L^+	$C_{80}H_{106}KN_{26}O_{22}^+$	1821.74	1821.7606
Na_2HL^+	$C_{80}H_{105}N_{26}Na_2O_{22}^+$	1827.75	1827.7687
$KNaHL^+$	$C_{80}H_{105}KN_{26}NaO_{22}^+$	1843.71	1843.7426
Na_2HL^+	$C_{80}H_{104}N_{26}Na_3O_{22}^+$	1849.73	1849.7506

Table A2. CD spectral parameters of the copper(II) complexes of multihistidine peptides (w = wide).

Species	Binding Mode	λ_{max} (nm) (ε (M^{-1} cm^{-1}))		
		$L^1(10)$	$L^2(15)$	$L^3(16)$
$[CuH_{-3}L]$	$[N^-, N^-, N^-, Im]$	659 (+0.989) 510 (−1.563) 410 (−0.068) 372 (−0.128) 332 (+0.547) 300 (−0.378) 261 (+6.341) w	748 (+0.064) w 606 (−0.684) 511 (+1.191) 348 (+0.097) 309 (−1.012) 278 (+1.309) 256 (+0.677)	718 (+0.127) 606 (−0.551) 513 (+0.966) 350 (+0.083) 309 (−0.997) 276 (+1.590) 259 (+1.059)
$[Cu_2H_{-6}L]$	$2 \times [N^-, N^-, N^-, Im]$	–	686 (+0.328) w 586 (−0.271) 516 (+0.144) 379 (−0.042) 339 (+0.286) 307 (−0.686) 266 (+3.060) 253 (+2.850)	678 (+0.538) 576 (−0.235) 496 (−0.112) 446 (+0.024) 374 (−0.085) 336 (+0.262) 306 (−0.792) 263 (+4.195)

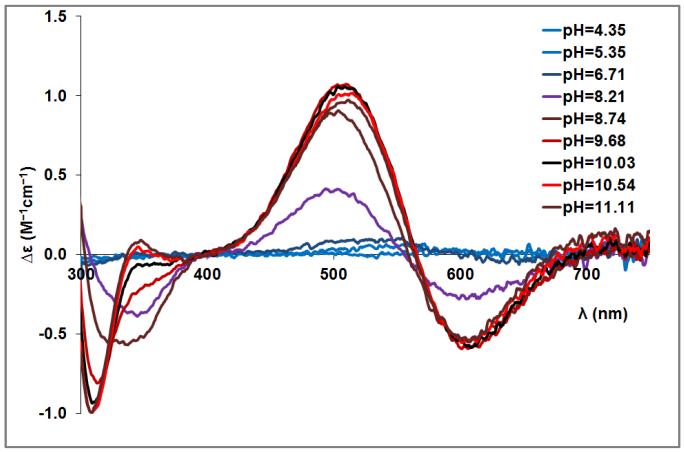

Figure A1. pH-dependent CD spectra of the Cu(II)-$L^3(16)$ system at 1:1 ratio ($c_{Cu(II)} = c_L = 0.7$ mM).

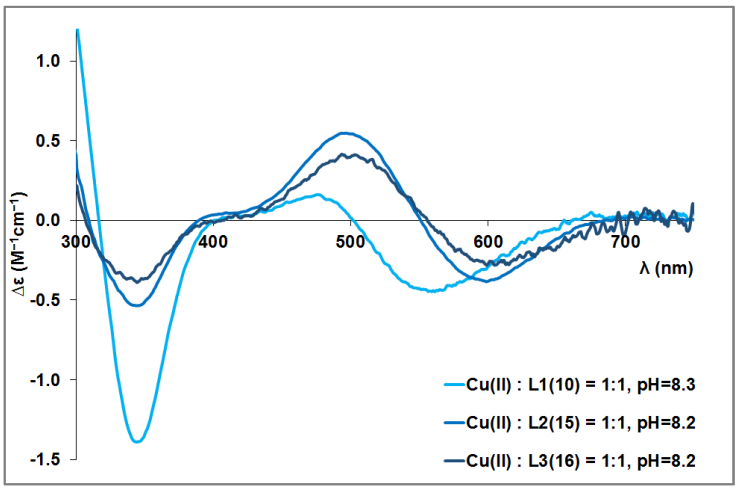

(**a**)

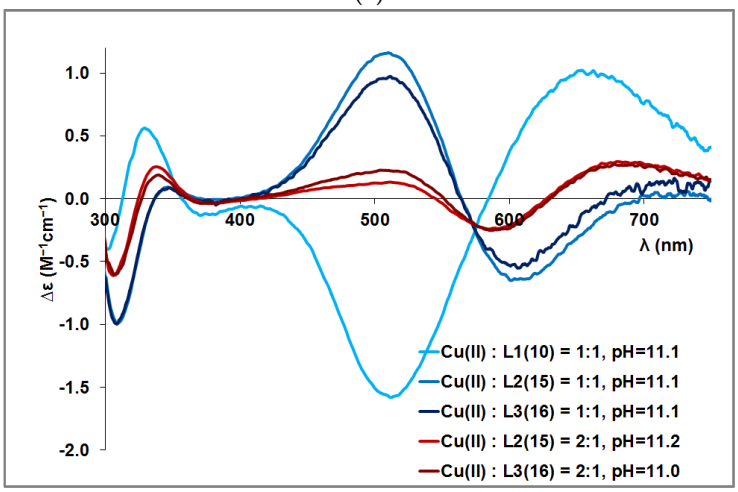

(**b**)

Figure A2. CD spectra of the copper(II) complexes of $L^1(10)$, $L^2(15)$, and $L^3(16)$ around pH 8 (**a**) and pH 11 (**b**) at Cu(II)-L = 1:1 and 2:1 ratios (c_L = 0.7 mM).

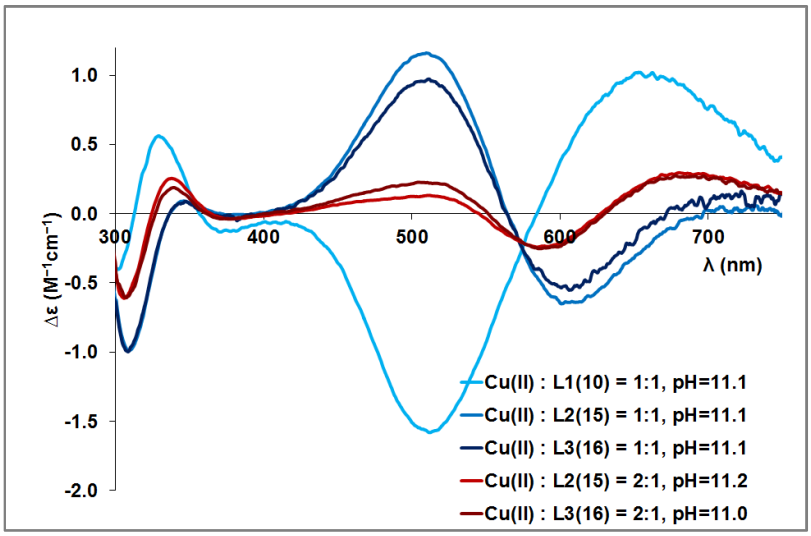

(**a**)

Figure A3. *Cont.*

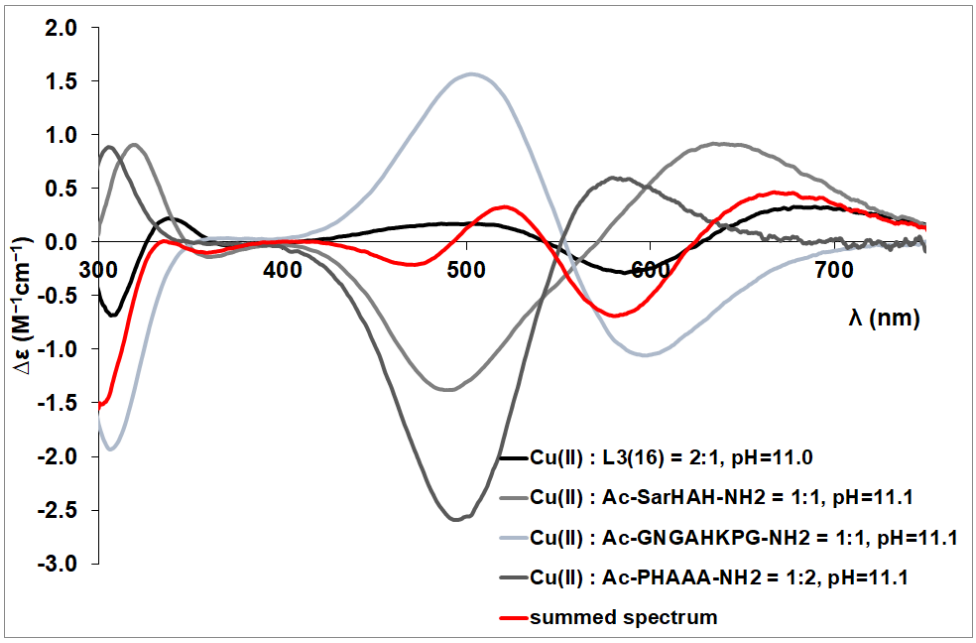

(**b**)

Figure A3. (**a**) CD spectra of the Cu(II)-L^3(16) (black), Cu(II)-Ac-SarHAH-NH_2, Cu(II)-Ac-GNGAHKPG-NH_2, and Cu(II)-Ac-PHAAA-NH_2 complexes and spectra obtained by summing the CD spectra of Cu(II)-Ac-SarHAH-NH_2, Cu(II)-Ac-GNGAHKPG-NH_2 and Cu(II)-Ac-PHAAA-NH_2 in 80%:5%:15% ratio (red) at pH ~11.1; (**b**) CD spectra of the Cu(II)-L^3(16), Cu(II)-Ac-SarHAH-NH_2, Cu(II)-Ac-GNGAHKPG-NH_2 and Cu(II)-Ac-PHAAA-NH_2 complexes and spectra obtained by summing the CD spectra of Cu(II)-Ac-SarHAH-NH_2, Cu(II)-Ac-GNGAHKPG-NH_2 and Cu(II)-Ac-PHAAA-NH_2 in 45%:50%:5% ratio (red) at pH ~11.1. Cu(II)-Ac-SarHAH-NH_2, Cu(II)-Ac-GNGAHKPG-NH_2 and Cu(II)-Ac-PHAAA-NH_2 in 45%:50%:5% ratio (red) at pH ~11.1.

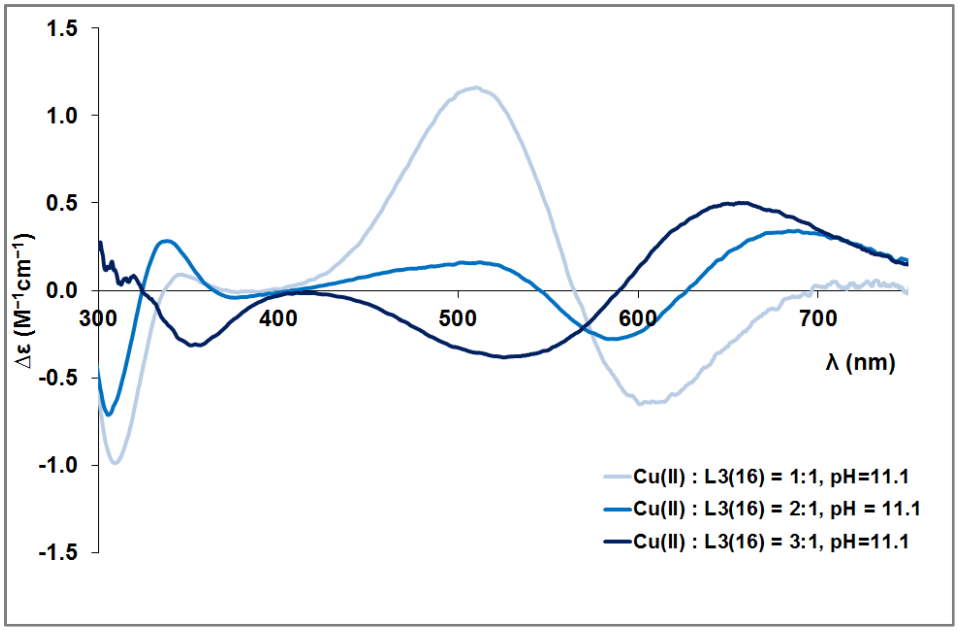

Figure A4. CD spectra registered at various Cu(II)-L^2(15) ratios at pH 11.

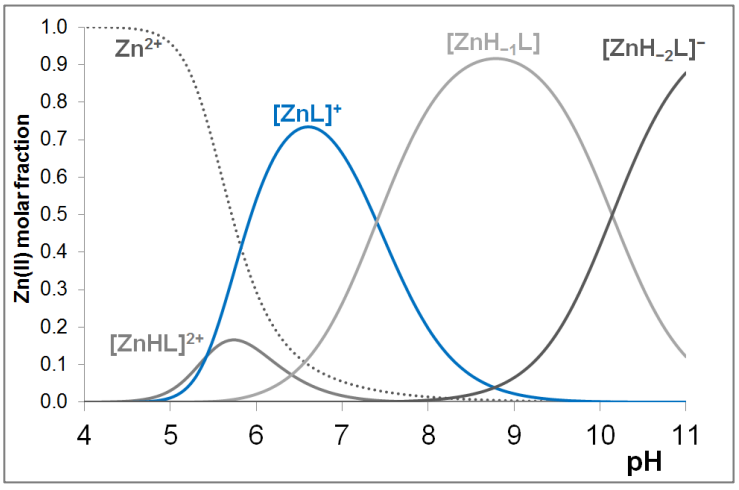

(**a**)

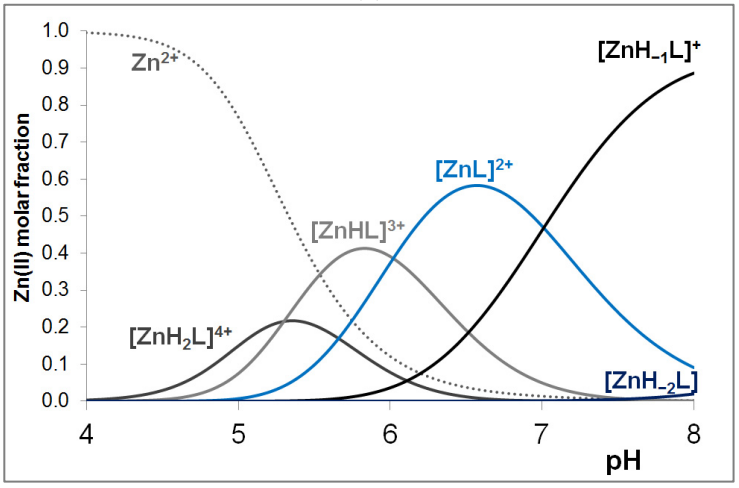

(**b**)

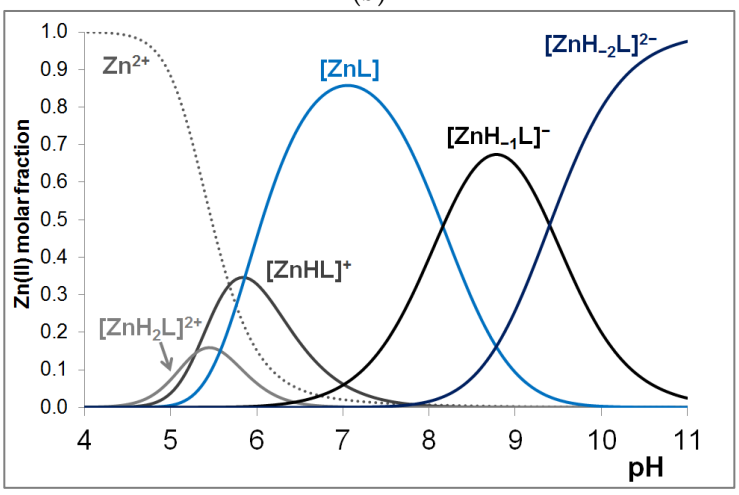

(**c**)

Figure A5. Distribution curves of complexes formed in the equimolar solution of Zn(II)-L^1(10) (**a**), Zn(II)-L^2(15) (**b**) and Zn(II)L^3(16) (**c**) ($c_L = c_M = 0.8$ mM).

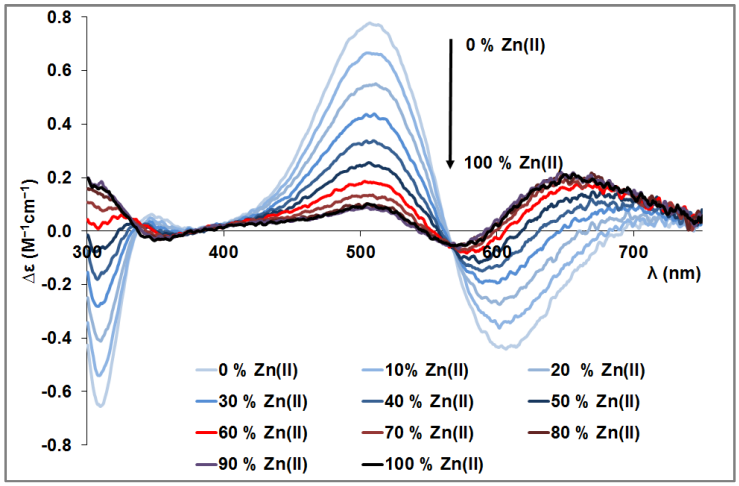

Figure A6. CD spectra registered in the Cu(II)-Zn(II)-L^3(16) system in the function of Zn(II) ($c_L = c_{Cu(II)}$ = 0.9 mM, pH = 11.2).

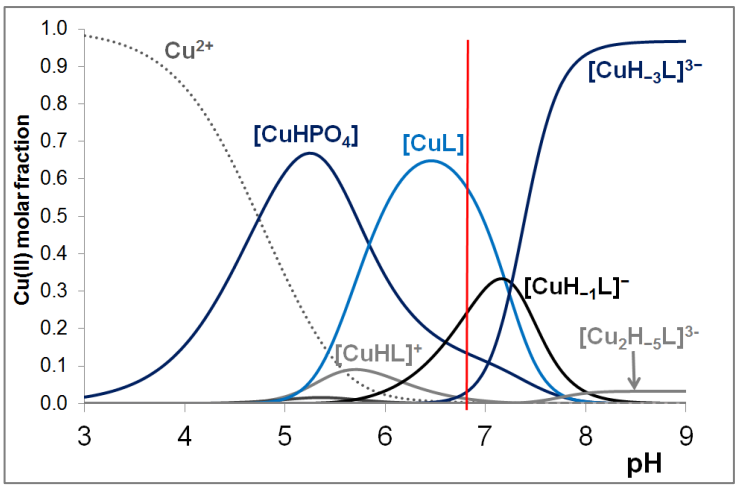

(**a**)

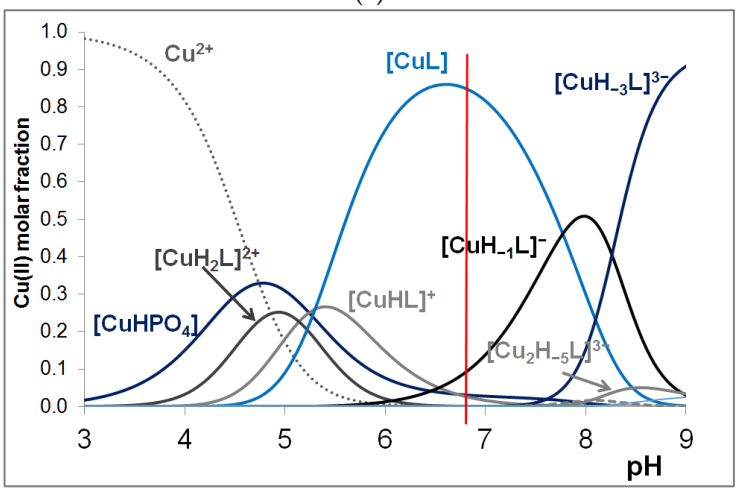

(**b**)

Figure A7. Distribution curves of complexes formed in the Cu(II)-L^2(15) (**a**) and Cu(II)-L^3(16) (**b**) system in the presence of $H_2PO_4^-$—HPO_4^{2-} buffer ($c_L = c_{Cu(II)} = 2 \times 10^{-3}$ mM; c_{buffer} = 50 mM).

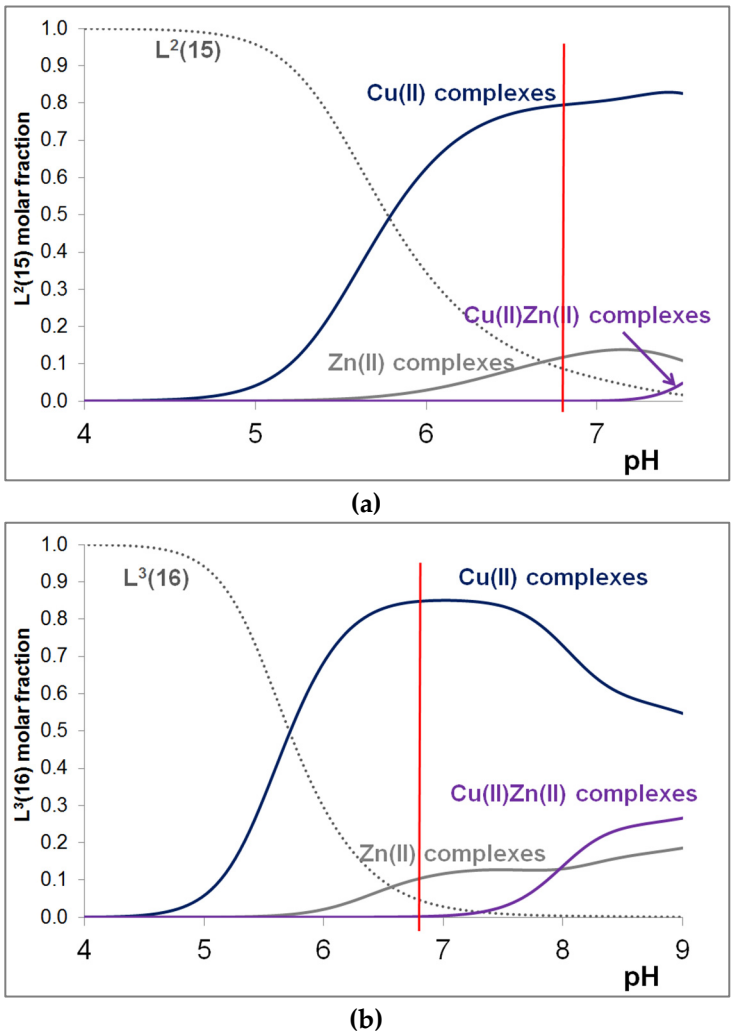

Figure A8. Distribution curves of complexes formed in the Cu(II)-Zn(II)-$L^2(15)$ (**a**) and Cu(II)-Zn(II)-$L^3(16)$ (**b**) system in the presence of $H_2PO_4^-$—HPO_4^{2-} buffer ($c_L = c_{Cu(II)} = c_{Zn(II)} = 2 \times 10^{-3}$ mM; c_{buffer} = 50 mM.

References

1. Fridovich, I. Fundamental aspects of reactive oxygen species, or what's the matter with oxygen. *Ann. N. Y. Acad. Sci.* **1999**, *893*, 13–18. [CrossRef] [PubMed]
2. Parkes, T.L.; Elia, A.J.; Dickinson, D.; Hilliker, A.J.; Phillips, J.P.; Boulianne, G.L. Extension of Drosophila lifespan by overexpression of human SOD1 in motorneurons. *Nat. Genet.* **1998**, *19*, 171–174. [CrossRef] [PubMed]
3. McCord, J.M.; Fridovich, I. Superoxide dismutase. An enzymic function for erythrocuprein (hemocuprein). *J. Biol. Chem.* **1969**, *244*, 6049–6055. [CrossRef] [PubMed]
4. Rosen, D.R.; Siddique, T.; Patterson, D.; Figlewicz, D.A.; Sapp, P.; Hentati, A.; Donaldson, D.; Goto, J.; O'Regan, J.P. Mutations in Cu/Zn superoxide dismutase gene are associated with familial amyotrophic lateral sclerosis. *Nature* **1993**, *362*, 59–62. [CrossRef] [PubMed]
5. Lyons, T.J.; Nersissian, A.; Huang, H.; Yeom, H.; Nishida, C.R.; Graden, J.A.; Butler Gralla, E.; Selverstone Valentine, J. The metal binding properties of the zinc site of yeast copper-zinc superoxide dismutase: Implications for amyotrophic lateral sclerosis. *J. Biol. Inorg. Chem.* **2000**, *5*, 189–203. [CrossRef] [PubMed]
6. Weiss, S.J.; King, G.W.; LoBuglio, A.F. Superoxide generation by human monocytes and macrophages. *Am. J. Hematol.* **1978**, *4*, 1–8. [CrossRef] [PubMed]
7. Mills, E.L.; Debets-Ossenkopp, Y.; Verbrugh, H.A.; Verhoef, J. Initiation of the respiratory burst of human neutrophils by influenza virus. *Infect. Immun.* **1981**, *32*, 1200–1205. [CrossRef] [PubMed]
8. Klug, D.; Rabani, J.; Fridovich, I. A direct demonstration of the catalytic action of superoxide dismutase through the use of pulse radiolysis. *J. Biol. Chem.* **1972**, *247*, 4839–4842. [CrossRef]

9. Schmidt, P.J.; Rae, T.D.; Pufahl, R.A.; Hamma, T.; Strain, J.; O'Halloran, T.V.; Culotta, V.C. Multiple protein domains contribute to the action of the copper chaperone for superoxide dismutase. *J. Biol. Chem.* **1999**, *274*, 23719–23725. [CrossRef]
10. Hall, L.T.; Sanchez, R.J.; Holloway, S.P.; Zhu, H.; Stine, J.E.; Lyons, T.J.; Demeler, B.; Schirf, V.; Hansen, J.C.; Nersissian, A.M.; et al. X-ray Crystallographic and analytical ultracentrifugation analyses of truncated and full-length yeast copper chaperones for SOD (LYS7): A dimer−dimer model of LYS7−SOD association and copper delivery. *Biochemistry* **2000**, *39*, 3611–3623. [CrossRef]
11. Torres, A.S.; Petri, V.; Rae, T.D.; O'Halloran, T.V. Copper stabilizes a heterodimer of the yCCS metallochaperone and its target superoxide dismutase. *J. Biol. Chem.* **2001**, *276*, 38410–38416. [CrossRef]
12. Lamb, A.L.; Torres, A.S.; O'Halloran, T.V.; Rosenzweig, A.C. Heterodimeric structure of superoxide dismutase in complex with its metallochaperone. *Nat. Struct. Biol.* **2001**, *8*, 751–755. [CrossRef] [PubMed]
13. Teoh, M.L.T.; Walasek, P.J.; Evans, H.D. *Leporipoxvirus* Cu,Zn-superoxide dismutase (SOD) homologs are catalytically inert decoy proteins that bind copper chaperone for SOD. *J. Biol. Chem.* **2003**, *278*, 33175–33184. [CrossRef] [PubMed]
14. Yount, N.Y.; Bayer, A.S.; Xiong, Y.Q.; Yeaman, M.R. Advances in antimicrobial peptide immunobiology. *Biopolymers* **2006**, *84*, 435–458. [CrossRef]
15. Pasupuleti, M.; Davoudi, M.; Malmsten, M.; Schmidtchen, A. Antimicrobial activity of a C-terminal peptide from human extracellular superoxide dismutase. *BMC Res. Notes* **2009**, *2*, 136. [CrossRef] [PubMed]
16. Steiner, H.; Hultmark, D.; Engstrom, A.; Bennich, H.; Boman, H.G. Sequence and specificity of two antibacterial proteins involved in insect immunity. *Nature* **1981**, *292*, 246–248. [CrossRef]
17. Zasloff, M. Magainins, a class of antimicrobial peptides from Xenopus skin: Isolation, characterization of two active forms, and partial cDNA sequence of a precursor. *Proc. Natl. Acad. Sci. USA* **1987**, *84*, 5449–54453. [CrossRef]
18. Gudmundsson, G.H.; Lidholm, D.A.; Asling, B.; Gan, R.; Boman, H.G. The cecropin locus. Cloning and expression of a gene cluster encoding three antibacterial peptides in Hyalophora cecropia. *J. Biol. Chem.* **1991**, *266*, 11510–11517. [CrossRef]
19. Agerberth, B.; Gunne, H.; Odeberg, J.; Kogner, P.; Boman, H.G.; Gudmundsson, G.H. FALL-39, a putative human peptide antibiotic, is cysteine-free and expressed in bone marrow and testis. *Proc. Natl. Acad. Sci. USA* **1995**, *92*, 195–199. [CrossRef]
20. Cowland, J.B.; Johnsen, A.H. Borregaard, hCAP-18, a cathelin/pro-bactenecin-like protein of human neutrophil specific granules. *FEBS Lett.* **1995**, *368*, 173–176. [CrossRef] [PubMed]
21. Douglas, S.E.; Gallant, J.W.; Gong, Z.; Hew, C. Cloning and developmental expression of a family of pleurocidin-like antimicrobial peptides from winter flounder, Pleuronectes americanus (Walbaum). *Dev. Comp. Immunol.* **2001**, *25*, 137–147. [CrossRef]
22. Wieprecht, T.; Beyermann, M.; Seelig, J. Thermodynamics of the coil-alpha-helix transition of amphipathic peptides in a membrane environment: The role of vesicle curvature. *Biophys. Chem.* **2002**, *96*, 191–201. [CrossRef] [PubMed]
23. Andersson, M.; Boman, A.; Boman, H.G. Ascaris nematodes from pig and human make three antibacterial peptides: Isolation of cecropin P1 and two ASABF peptides. *Cell. Mol. Life Sci.* **2003**, *60*, 599–606. [CrossRef] [PubMed]
24. Lequin, O.; Bruston, F.; Convert, O.; Chassaing, G.; Nicolas, P. Helical structure of dermaseptin B2 in a membrane-mimetic environment. *Biochemistry* **2003**, *42*, 10311–10323. [CrossRef]
25. Pukala, T.L.; Brinkworth, C.S.; Carver, J.A.; Bowie, J.H. Investigating the importance of the flexible hinge in caerin 1.1: Solution structures and activity of two synthetically modified caerin peptides. *Biochemistry* **2004**, *43*, 937–944. [CrossRef]
26. Syvitski, R.T.; Burton, I.; Mattatall, N.R.; Douglas, S.E.; Jakeman, D.L. Structural characterization of the antimicrobial peptide pleurocidin from winter flounder. *Biochemistry* **2005**, *44*, 7282–7293. [CrossRef] [PubMed]
27. Tang, Y.Q.; Yuan, J.; Osapay, G.; Osapay, K.; Tran, D.; Miller, C.J.; Ouellette, A.J.; Selsted, M.E. A cyclic antimicrobial peptide produced in primate leukocytes by the ligation of two truncated α-defensins. *Science* **1999**, *286*, 498–502. [CrossRef]
28. Yount, N.Y.; Yeaman, M.R. Multidimensional signatures in antimicrobial peptides. *Proc. Natl. Acad. Sci. USA* **2004**, *101*, 7363–7368. [CrossRef]
29. Ganz, T. Defensins and other antimicrobial peptides: A historical perspective and an update. *Comb. Chem. High. Throughput Screen* **2005**, *8*, 209–217. [CrossRef]
30. Wieprecht, T.; Apostolov, O.; Beyermann, M.; Seelig, J. Thermodynamics of the α-helix-coil transition of amphipathic peptides in a membrane environment: Implications for the peptide-membrane binding equilibrium. *J. Mol. Biol.* **1999**, *294*, 785–794. [CrossRef]
31. Marshall, S.H. Antimicrobial peptides: A natural alternative to chemical antibiotics and a potential for applied biotechnology. *Electron. J. Biotechnol.* **2003**, *6*, 3. [CrossRef]
32. Brogden, K.A. Antimicrobial peptides: Pore formers or metabolic inhibitors in bacteria? *Nat. Rev. Microbiol.* **2005**, *3*, 238–250. [CrossRef]
33. Andersson, E.; Rydengård, V.; Sonesson, A.; Mörgelin, M.; Björck, L.; Schmidtchen, A. Antimicrobial activities of heparin-binding peptides. *Eur. J. Biochem.* **2004**, *271*, 1219–1226. [CrossRef]
34. Nordahl, E.A.; Rydengård, V.; Nyberg, P.; Nitsche, D.P.; Mörgelin, M.; Malmsten, M.; Björck, L.; Schmidtchen, A. Activation of the complement system generates antibacterial peptides. *Proc. Natl. Acad. Sci. USA* **2004**, *101*, 16879–16884. [CrossRef] [PubMed]
35. Pasupuleti, M.; Walse, B.; Nordahl, E.A.; Morgelin, M.; Malmsten, M.; Schmidtchen, A. Preservation of antimicrobial properties of complement peptide C3a, from invertebrates to humans. *J. Biol. Chem.* **2007**, *282*, 2520–2528. [CrossRef] [PubMed]
36. Nordahl, E.A.; Rydengård, V.; Mörgelin, M.; Schmidtchen, A. Domain 5 of high molecular weight kininogen is antibacterial. *J. Biol. Chem.* **2005**, *280*, 34832–34839. [CrossRef] [PubMed]
37. Malmsten, M.; Davoudi, M.; Schmidtchen, A. Bacterial killing by heparin-binding peptides from PRELP and thrombospondin. *Matrix Biol.* **2006**, *25*, 294–300. [CrossRef] [PubMed]

38. Malmsten, M.; Davoudi, M.; Walse, B.; Rydengard, V.; Pasupuleti, M.; Morgelin, M.; Schmidtchen, A. Antimicrobial peptides derived from growth factors. *Growth Factors* **2007**, *25*, 60–70. [CrossRef] [PubMed]
39. Oppenheim, F.G.; Xu, T.; McMillian, F.M.; Levitz, S.M.; Diamond, R.D.; Offner, G.D.; Troxler, R.F. Histatins, a novel family of histidine-rich proteins in human parotid secretion.Isolation, characterization, primary structure, and fungistatic effects on Candida albicans. *J. Biol. Chem.* **1988**, *263*, 7472–7477. [CrossRef]
40. Frank, R.W.; Gennaro, R.; Schneider, K.; Przybylski, M.; Romeo, D. Amino acid sequences of two proline-rich bactenecins. Antimicrobial peptides of bovine neutrophils. *J. Biol. Chem.* **1990**, *265*, 18871–18874. [CrossRef] [PubMed]
41. Selsted, M.E.; Novotny, M.J.; Morris, W.L.; Tang, Y.Q.; Smith, W.; Cullor, J.S. Indolicidin, a novel bactericidal tridecapeptide amide from neutrophils. *J. Biol. Chem.* **1992**, *267*, 4292–4295. [CrossRef] [PubMed]
42. Cabiaux, V.; Agerberth, B.; Johansson, J.; Homble, F.; Goormaghtigh, E.; Ruysschaert, J.M. Secondary structure and membrane interaction of PR-39, a Pro+ Arg-rich antibacterial peptide. *Eur. J. Biochem.* **1994**, *224*, 1019–1027. [CrossRef]
43. Gudmundsson, G.H.; Magnusson, K.P.; Chowdhary, B.P.; Johansson, M.; Andersson, L.; Boman, H.G. Structure of the gene for porcine peptide antibiotic PR-39, a cathelin gene family member: Comparative mapping of the locus for the human peptide antibiotic FALL-39. *Proc. Natl. Acad. Sci. USA* **1995**, *92*, 7085–7089. [CrossRef] [PubMed]
44. Schibli, D.J.; Hwang, P.M.; Vogel, H.J. Structure of the antimicrobial peptide tritrpticin bound to micelles: A distinct membrane-bound peptide fold. *Biochemistry* **1999**, *38*, 16749–16755. [CrossRef]
45. Rozek, A.; Friedrich, C.L.; Hancock, R.E. Structure of the bovine antimicrobial peptide indolicidin bound to dodecylphosphocholine and sodium dodecyl sulfate micelles. *Biochemistry* **2000**, *39*, 15765–15774. [CrossRef]
46. Rydengard, V.; Olsson, A.K.; Morgelin, M.; Schmidtchen, A. Histidinerich glycoprotein exerts antibacterial activity. *FEBS J.* **2007**, *274*, 377–389. [CrossRef] [PubMed]
47. Rydengard, V.; Shannon, O.; Lundqvist, K.; Kacprzyk, L.; Chalupka, A.; Olsson, A.K.; Morgelin, M.; Jahnen-Dechent, W.; Malmsten, M.; Schmidtchen, A. Histidine-rich glycoprotein protects from systemic Candida infection. *PLoS Pathog.* **2008**, *4*, e1000116. [CrossRef]
48. Frueh, J.; Gai, M.; Yang, Z.; He, Q. Influence of Polyelectrolyte Multilayer Coating on the Degree and Type of Biofouling in Freshwater Environment. *J. Nanosci. Nanotechnol.* **2014**, *14*, 4341–4350. [CrossRef]
49. Badaraev, A.D.; Lerner, M.I.; Bakina, O.V.; Sidelev, D.V.; Tran, T.-H.; Krinitcyn, M.G.; Malashicheva, A.B.; Cherempey, E.G.; Slepchenko, G.B.; Kozelskaya, A.I.; et al. Antibacterial Activity and Cytocompatibility of Electrospun PLGA Scaffolds Surface-Modified by Pulsed DC Magnetron Co-Sputtering of Copper and Titanium. *Pharmaceutics* **2023**, *15*, 939. [CrossRef]
50. Suksrichavalit, T.; Prachayasittikul, S.; Nantasenamat, C.; Isarankura-NaAyudhya, C.; Prachayasittikul, V. Copper complexes of pyridine derivatives with superoxide scavenging and antimicrobial activities. *Eur. J. Med. Chem.* **2009**, *44*, 3259–3265. [CrossRef]
51. Mehta, J.V.; Gajera, S.B.; Patel, M.N. Antimalarial, antimicrobial, cytotoxic, DNA interaction and SOD like activities of tetrahedral copper(II) complexes. *Spectrochim. Acta A Mol. Biomol. Spectrosc.* **2015**, *136*, 1881–1892. [CrossRef]
52. Joseph, J.; Boomadevi Janaki, G.; Nagashri, K.; Selwin Joseyphus, R. Antimicrobial, antioxidant and SOD activities of copper(II) complexes derived from 2-aminobenzothiazole derivatives. *J. Coord. Chem.* **2017**, *70*, 242–260. [CrossRef]
53. Csire, G.; Timári, S.; Asztalos, J.; Király, J.M.; Kiss, M.; Várnagy, K. Coordination, redox properties and SOD activity of Cu(II) complexes of multihistidine peptides. *J. Inorg. Biochem.* **2017**, *177*, 198–210. [CrossRef] [PubMed]
54. Grenács, Á.; Kaluha, A.; Kállay, C.; Jószai, V.; Sanna, D.; Sóvágó, I. Binary and ternary mixed metal complexes of terminally free peptides containing two different histidyl binding sites. *J. Inorg. Biochem.* **2013**, *128*, 17–25. [CrossRef] [PubMed]
55. Raics, M.; Sanna, D.; Sóvágó, I.; Kállay, C. Copper(II), nickel(II) and zinc(II) complexes of hexapeptides containing separate aspartyl and histidyl residues. *Inorg. Chim. Acta* **2015**, *426*, 99–106. [CrossRef]
56. Csire, G.; Nagy, L.; Várnagy, K.; Kállay, C. Copper(II) interaction with the Human Prion 103-112 fragment-Coordination and oxidation. *J. Inorg. Biochem.* **2017**, *170*, 195–201. [CrossRef] [PubMed]
57. Irving, H.M.; Miles, M.G.; Pettit, L.D. A study of some problems in determining the stoicheiometric proton dissociation constants of complexes by potentiometric titrations using a glass electrode. *Anal. Chim. Acta* **1967**, *38*, 475–488. [CrossRef]
58. Gans, P.; Sabatini, A.; Vacca, A. SUPERQUAD: An improved general program for computation of formation constants from potentiometric data. *J. Chem. Soc. Dalton Trans.* **1985**, *6*, 1195–1200. [CrossRef]
59. Zékány, L.; Nagypál, I. *Computational Methods for the Determination of Formation Constants*; Leggett, D.J., Ed.; Plenum Press: New York, NY, USA, 1985; pp. 291–353.
60. Beauchamp, C.; Fridovich, I. Superoxide dismutase: Improved assays and an assay applicable to acrylamide gels. *Anal. Biochem.* **1974**, *44*, 276–287. [CrossRef]
61. Goldstein, S.; Michel, C.; Bors, W.; Saran, M.; Czapski, G. A critical reevaluation of some assay methods for superoxide dismutase activity. *Free Radic. Biol. Med.* **1988**, *4*, 295–303. [CrossRef]
62. Durot, S.; Policar, C.; Cisnetti, F.; Lambert, F.; Renault Pelosi, G.; Blain, G.; Korri-Youssoufi, H.; Mahy, J.-P. Series of Mn complexes based on N-centered ligands and superoxide−reactivity in an anhydrous medium and SOD-like activity in an aqueous medium correlated to Mn II/Mn III redox potentials. *Eur. J. Inorg. Chem.* **2005**, *2005*, 3513–3523. [CrossRef]
63. Székely, E.; Csire, G.; Balogh, B.D.; Erdei, J.Z.; Király, J.M.; Kocsi, J.; Pinkóczy, J.; Várnagy, K. The role of side chains in the fine-tuning of the metal-binding ability of multihistidine peptides. *Molecules* **2022**, *27*, 3435. [CrossRef]

64. Kállay, C.; Várnagy, K.; Malandrinos, G.; Hadjiliadis, N.; Sanna, D.; Sóvágó, I. Thermodynamic and structural characterization of the macrochelates formed in the reactions of copper(II) and zinc(II) ions with peptides of histidine. *Inorg. Chim. Acta* **2009**, *362*, 935–945. [CrossRef]
65. Lukács, M.; Szunyog, G.; Grenács, Á.; Lihi, N.; Kállay, C.; Di Natale, G.; Campagna, T.; Lanza, V.; Tabbi, G.; Pappalardo, G.; et al. Copper(II) coordination abilities of the *tau* protein's N-terminus peptide fragments: A combined potentiometric, spectroscopic and mass spectrometric study. *Chem. Plus Chem.* **2019**, *84*, 1697–1708. [CrossRef]
66. Billo, E. Copper(II) chromosomes and the rule of average environment. *J. Inorg. Nucl. Chem. Lett.* **1974**, *10*, 613–617. [CrossRef]
67. Jószai, V.; Nagy, Z.; Ősz, K.; Sanna, D.; Di Natale, G.; La Mendola, D.; Pappalardo, G.; Rizzarelli, E.; Sóvágó, I. Transition metal complexes of terminally protected peptides containing histidyl residues. *J. Inorg. Biochem.* **2006**, *100*, 1399–1409. [CrossRef] [PubMed]
68. Csire, G.; Turi, I.; Sóvágó, I.; Kárpáti, E.; Kállay, C. Complex formation processes and metal ion catalyzed oxidation of model peptides related to the metal binding site of the human prion protein. *J. Inorg. Biochem* **2020**, *203*, 110927. [CrossRef]
69. Ohtsu, H.; Shimazaki, Y.; Odani, A.; Yamauchi, O.; Mori, W.; Itoh, S.; Fukuzumi, S. Synthesis and characterization of imidazolate-bridged dinuclear complexes as active site models of Cu,Zn-SOD. *J. Am. Chem. Soc.* **2000**, *122*, 5733–5741. [CrossRef]
70. Diószegi, R.; Bonczidai-Kelemen, D.; Bényei, A.C.; May, N.V.; Fábián, I.; Lihi, N. Copper(II) complexes of pyridine-2,6-dicarboxamide ligands with high SOD activity. *Inorg. Chem.* **2022**, *61*, 2319–2332. [CrossRef] [PubMed]
71. Kachadourian, R.; Batinic-Haberle, I.; Fridovich, I. Syntheses and superoxide dismuting activities of partially (1−4) β-chlorinated derivatives of manganese(III) *meso*-tetrakis(*N*-ethylpyridinium-2-yl)porphyrin. *Inorg. Chem.* **1999**, *38*, 391–396. [CrossRef]